Photochemical & Photobiological Sciences (2024) 23:539–560
https://doi.org/10.1007/s43630-024-00538-1

ORIGINAL PAPERS

Refining antimicrobial photodynamic therapy: effect of charge distribution and central metal ion in fluorinated porphyrins on effective control of planktonic and biofilm bacterial forms

Barbara Pucelik[1,2,3] · Agata Barzowska[2,4] · Adam Sułek[1,3] · Mateusz Werłos[1] · Janusz M. Dąbrowski[1]

Received: 3 November 2023 / Accepted: 13 January 2024 / Published online: 8 March 2024

Abstract

Antibiotic resistance represents a pressing global health challenge, now acknowledged as a critical concern within the framework of One Health. Photodynamic inactivation of microorganisms (PDI) offers an attractive, non-invasive approach known for its flexibility, independence from microbial resistance patterns, broad-spectrum efficacy, and minimal risk of inducing resistance. Various photosensitizers, including porphyrin derivatives have been explored for pathogen eradication. In this context, we present the synthesis, spectroscopic and photophysical characteristics as well as antimicrobial properties of a palladium(II)-porphyrin derivative (PdF_2POH), along with its zinc(II)- and free-base counterparts (ZnF_2POH and F_2POH, respectively). Our findings reveal that the palladium(II)-porphyrin complex can be classified as an excellent generator of reactive oxygen species (ROS), encompassing both singlet oxygen ($\Phi_\Delta = 0.93$) and oxygen-centered radicals. The ability of photosensitizers to generate ROS was assessed using a variety of direct (luminescence measurements) and indirect techniques, including specific fluorescent probes both in solution and in microorganisms during the PDI procedure. We investigated the PDI efficacy of F_2POH, ZnF_2POH, and PdF_2POH against both Gram-negative and Gram-positive bacteria. All tested compounds proved high activity against Gram-positive species, with PdF_2POH exhibiting superior efficacy, leading to up to a 6-log reduction in *S. aureus* viability. Notably, PdF_2POH-mediated PDI displayed remarkable effectiveness against *S. aureus* biofilm, a challenging target due to its complex structure and increased resistance to conventional treatments. Furthermore, our results show that PDI with PdF_2POH is more selective for bacterial than for mammalian cells, particularly at lower light doses (up to 5 J/cm^2 of blue light illumination). This enhanced efficacy of PdF_2POH-mediated PDI as compared to ZnF_2POH and F_2POH can be attributed to more pronounced ROS generation by palladium derivative via both types of photochemical mechanisms (high yields of singlet oxygen generation as well as oxygen-centered radicals). Additionally, PDI proved effective in eliminating bacteria within *S. aureus*-infected human keratinocytes, inhibiting infection progression while preserving the viability and integrity of infected HaCaT cells. These findings underscore the potential of metalloporphyrins, particularly the Pd(II)-porphyrin complex, as promising photosensitizers for PDI in various bacterial infections, warranting further investigation in advanced infection models.

✉ Barbara Pucelik
barbara.pucelik@uj.edu.pl

✉ Janusz M. Dąbrowski
jdabrows@chemia.uj.edu.pl

1 Faculty of Chemistry, Jagiellonian University, Kraków, Poland

2 Malopolska Centre of Biotechnology, Jagiellonian University, Kraków, Poland

3 Sano Centre for Computational Medicine, Kraków, Poland

4 Doctoral School of Exact and Natural Sciences, Jagiellonian University, Kraków, Poland

Graphical abstract

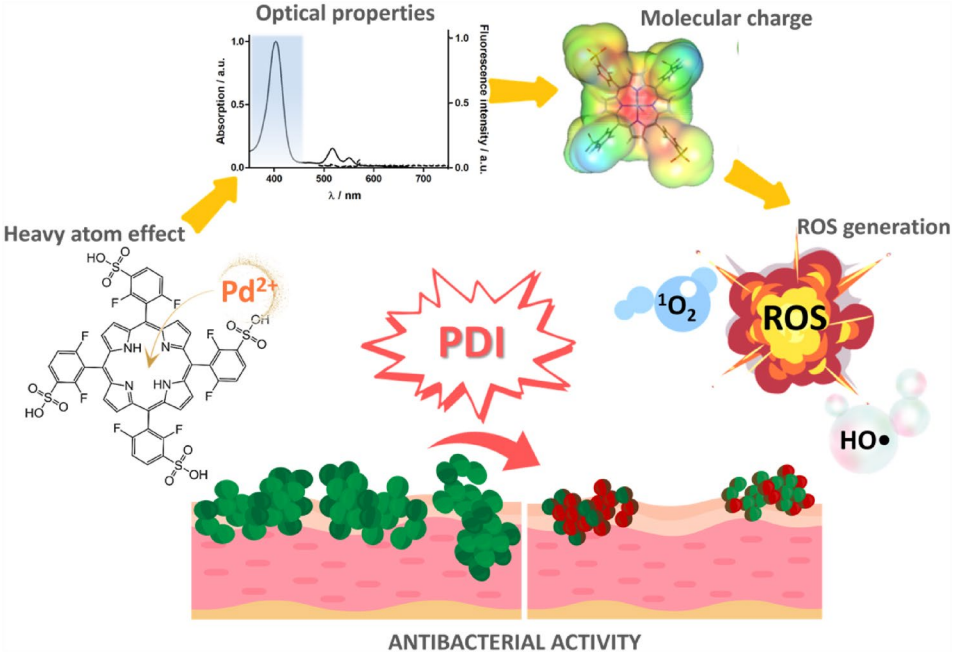

Keywords Biofilm · Metalloporphyrin · Photodynamic inactivation (PDI) · Photosensitizer · Porphyrin · Reactive oxygen species (ROS) · Singlet oxygen

1 Introduction

Antibiotic resistance of microorganisms stands as a pressing global health challenge, and it is indicated as a critical One Health issue [1]. The spread of antibiotic-resistant microorganisms can be attributed to various factors, including improper antibiotic use in both animals and humans, environmental pollution, and inadequate infection control measures. Consequently, it is conceivable that future pandemics may not necessarily arise from viral agents like SARS-CoV-2, responsible for COVID-19, but could potentially be triggered by other threatening pathogens, such as multidrug-resistant bacteria or microorganisms associated with issues related to water and food safety. Bacterial infections are a primary contributor to morbidity and mortality worldwide, especially in developing countries. The World Health Organization (WHO) indicates microbial resistance constitutes a worldwide menace, leading to an annual toll of approximately 50,000 lives in Europe and the US, as well as a substantial number of individuals across the globe. It is predicted that by the year 2050, microbial infections will surpass cancer as the leading cause of mortality globally [2].

The growing resistance of clinically important microorganisms such as *Escherichia*, *Pseudomonas*, and *Staphylococcus* represents a major clinical challenge in nosocomial environments. The rising emergence and dissemination of antibiotic-resistant and multidrug-resistant bacteria presents a significant danger to the public health and challenge the efficacy of conventional antibiotic therapy [3, 4]. For instance, patients diagnosed with *methicillin-resistant Staphylococcus aureus* (MRSA) infections are 64% more likely to die than those with drug-sensitive infections [2]. Antibiotic resistance can result from various mechanisms, such as mutation, gene transfer, efflux pumps, biofilm formation, and adaptive responses [5]. Given the limited introduction of new antibiotics into the arsenal of antimicrobial treatments in recent years, antibiotic resistance poses a significant health risk and contributes to the escalation of treatment expenses. Therefore, alternative or complementary strategies are needed to combat bacterial infections, especially those involving biofilms or chronic wounds. Numerous strategies encompass novel therapeutic methods like gene therapy, phage therapy, photobiostimulation, photothermal, and photodynamic treatments aimed at enhancing wound management [6, 7]. Among these strategies, photodynamic inactivation (PDI) offers a substantial edge over traditional treatments. The key advantage of PDI is its capacity to eliminate bacteria, irrespective of their resistance status. PDI is a promising technique that uses light-activated drugs known as

photosensitizers (PS) to generate reactive oxygen species (ROS), such as oxygen-centered radicals (Type I photochemical mechanism) and singlet oxygen ($^1O_2$) (Type II mechanism). These ROS can eliminate bacteria by damaging their essential components, such as DNA, proteins, and lipids. PDI has several advantages over antibiotic therapy, such as broad-spectrum activity, low toxicity to mammalian cells, and minimal side effects [8]. PDI can be applied to treat various bacterial infections, especially those involving the skin, such as acne, wounds and viral infections [9, 10]. Furthermore, it is noteworthy that there have been no reported instances of resistance developing against the photosensitizers used in this approach to combat microorganisms [8, 11–15]. The nature of PS and its ability to generate ROS are determining factors for the efficiency of PDI. Among the photosensitizers currently under investigation with potential use in PDI, porphyrins deserve particular attention. They are regarded as molecules with high potential for application in photomedicine due to their desired optical and photophysical properties as well as negligible cytotoxic effects in human cells [16]. Furthermore, porphyrins, along with their dihydro- and tetrahydro- derivatives, have been investigated in vitro and in vivo studies as potential antimicrobial agents effective against both Gram-positive and Gram-negative bacteria [17–19]. One of the most common ways to increase the water solubility of hydrophobic molecules is to attach sulfonic groups to the phenyl rings of the macrocycle. It further appears that these substituents increase their affinity for Gram-positive bacterial membranes [20, 21]. The introduction of halogen substituents into the porphyrin structure can also modulate its physicochemical and pharmacokinetic properties [22]. In particular, fluorine atoms can affect the lipophilicity and electron-withdrawing ability of tetrapyrroles, which contribute to their aggregation behavior, (photo)stability, fluorescence and singlet oxygen quantum yields as well as cellular uptake and biological activity [23–27].

Multiple studies have indicated that metalation represents a promising strategy for modifying the chemical and biological features of PDT photosensitizers. The choice of various metal ions also offers precise control over photochemical and electrochemical properties [16]. Within the realm of metalloporphyrin derivatives, complexes with metal ions like Pt^{2+}, Pd^{2+}, or Zn^{2+} are particularly intriguing as photosensitizers due to their high quantum yield of the triplet excited state—the precursor of ROS [28–32]. In our previous investigations, we synthesized a series of porphyrin derivatives and their metal complexes and explored how different metal ions influence their singlet oxygen quantum yield (Φ_Δ) [28, 33]. Among several classes of metalloporphyrins examined, zinc(II) complexes exhibited significantly higher Φ_Δ when compared to free base porphyrins, primarily attributed to the heavy atom effect. As for palladium(II) complexes, the most noteworthy is TOOKAD® Soluble (Padeliporfin, Skatel, WST11), a pioneering third-generation photosensitizer developed by Steba Biotech for the treatment of low-risk prostate cancer by vascular targeted photodynamic therapy (V-PDT). Chemically, it is a negatively charged semisynthetic derivative of the photosynthetic pigment Bacteriochlorophyll α (Bchl) [34, 35].

Numerous tetrapyrrole derivatives with diverse structural modifications have been developed for the purpose of targeting and deactivating various types of pathogens (i.e., bacteria, fungi, viruses and parasites). In the context of antibacterial activity, Gram-negative bacteria possess a distinctive membrane characterized by low permeability, rendering them more resilient to eradication compared to Gram-positive bacteria. Photosensitizers with a neutral or negatively charged profile, which effectively deactivate Gram-positive bacteria, exhibit limited or no effectiveness against Gram-negative bacteria. Conversely, photosensitizers featuring positive charges disrupt and increase permeability in both Gram-positive and Gram-negative membranes, resulting in the efficient photo-induced inactivation of these bacteria [8, 36]. The efficacy of this process is significantly influenced by the chemical properties of PS and the resistance mechanisms employed by bacteria, such as efflux pumps. However, it is important to note that smaller cationic photosensitizers may be prone to passive diffusion into host cells, potentially leading to heightened toxicity towards normal cells [37]. However, despite the promising outcomes achieved in the realm of PDI, it is imperative to explore effective strategies for enhancing its efficacy, selectivity, and reliability. Numerous indications suggest that the introduction of fluorine atoms [38], or the conjugation with saccharides, e.g., cyclodextrins [39, 40] and peptides [41, 42], especially those positively charged under physiological pH values, can notably augment the overall photophysical properties and photodynamic efficiency of porphyrins. Exciting perspectives have been recently opened by the preparation of porphyrin-based materials [43], porphyrinic formulations [44] and their combination with potassium iodide [45], that can effectively produce ROS while simultaneously enhancing the effectiveness of light-triggered antimicrobial agents.

Our previous work described the photophysical properties and the antimicrobial activity of a series of chlorinated porphyrin derivatives as well as some anthraquinone dyes impregnated on the surface of TiO_2 [46]. These compounds, along with T_4MPyP serving as a positively charged reference, were evaluated as antimicrobial photosensitizers against Gram-positive *Staphylococcus aureus* and Gram-negative *Escherichia coli* bacteria [47, 48].

In this work, we present a new fluorinated and sulfonated palladium porphyrin (PdF_2POH), compared with structurally related photosensitizers (F_2POH and ZnF_2POH). We

focus on their blue light-induced antimicrobial activity under conditions close to the normal living environment of bacteria, such as bacterial biofilm. Finally, we present for the first time an in vitro model of bacterial infection of human skin cells (HaCaT) and demonstrate high PDI efficiency in killing bacteria in infected skin cells using PdF_2POH as photosensitizer.

2 Results

2.1 Synthesis of metalloporphyrins

The general synthesis method for the *meso*-substituted porphyrin derivatives, including 5,10,15,20-tetrakis(2,6-difluoro-3-sulfophenyl)porphyrin (F_2POH), has been previously described [23]. The ZnF_2POH was used in our studies for modification of TiO_2 (P25) and $qTiO_2$, but its synthesis was not described in detail [47, 48]. To obtain F_2POH metal complexes, we started by synthesizing tetraphenylporphyrin precursors using a modified Adler-Longo method involving heating pyrrole **1** and 2,6-difluorobenzaldehyde **2** at boiling point (Fig. 1) [49]. Chlorosulfonic groups were then introduced into fluorinated tetraphenylporphyrin **3** using chlorosulfonic acid [50]. Next, the 5,10,15,20-tetrakis(2,6-difluoro-3-chlorosulfonyl) porphyrin **4**, was used to obtain metalloporphyrins via insertion of Pd(II) and Zn(II). The procedure involved a reaction between compound **4** with the suitable metal salt according to modified method described by He et al. [51], followed by hydrolysis to obtain the sulfonated derivatives. This approach significantly simplifies the process of purification because the presence of the chlorosulfonic groups makes the compound insoluble in water, and therefore the process of getting rid of the excess metal salt used is limited to extracting the product and washing it with water. The synthesis of ZnF_2POH **5** required the reaction of **4** with $Zn(OAc)_2$ in DCM/MeOH for 2 h at room temperature. Whereas the synthesis of PdF_2POH **6** involved reaction with $Pd(OAc)_2$ in DCM for 48 h at 40 °C (Fig. 1). The products were obtained with high yields of 90% and 86% for ZnF_2POH and PdF_2POH, respectively. The process of metalation was monitored by electronic absorption spectroscopy, and the end of the reaction was the replacement of the four Q bands for free-base porphyrin, with two Q bands characteristic for metalloporphyrins (change in symmetry between the two forms and the degeneracy of the LUMO orbital for porphyrin coordinated by the metal ion). Hydrolysis of F_2POH (free base, $M = 2H$), ZnF_2POH, and PdF_2POH consisted of heating them in water at boiling temperature for approximately 12 h. This slow hydrolysis method does not require the use of any catalyst, which would force an additional method of purifying the product. After completion of the reaction confirmed by TLC analysis, the overall mixture was concentrated using an evaporator, and the product was precipitated with acetone and isolated by filtration and drying. Structures of all products were confirmed by electronic absorption spectra, ^1H

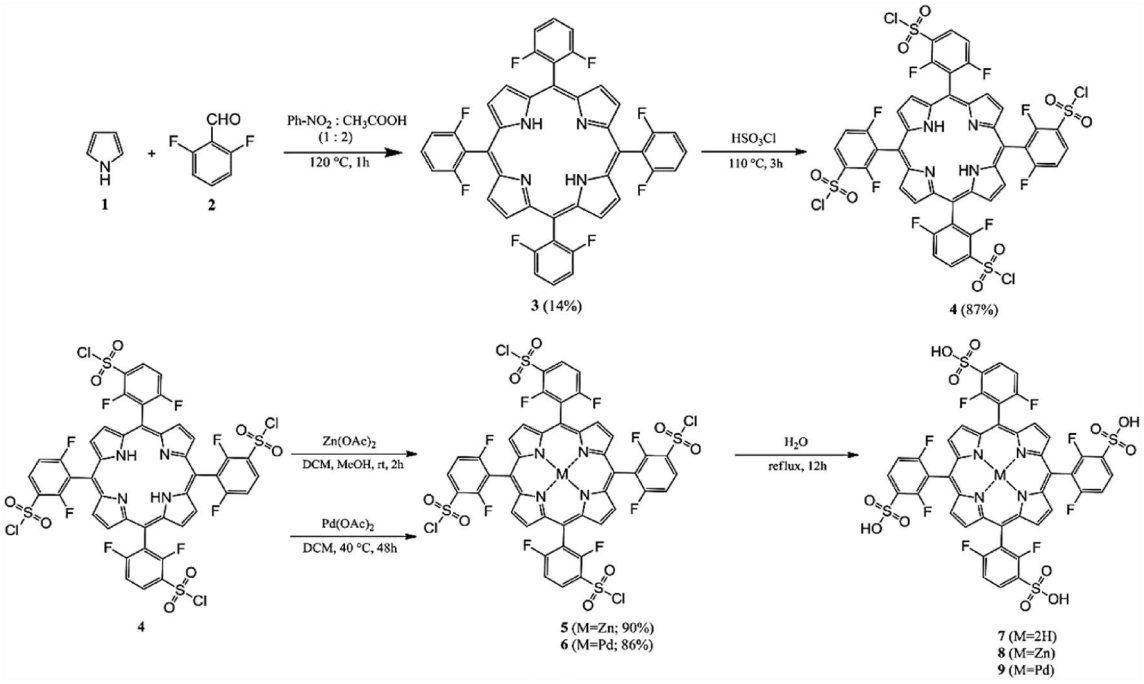

Fig. 1 Scheme of the synthesis of F_2POH and its metal complexes - ZnF_2POH and PdF_2POH, through following subsequent reaction steps

NMR spectra (no signals from N–H protons for ZnF_2POH and PdF_2POH relative to the compound F_2POH), and by elemental analysis.

2.2 Optical and photochemical properties

The electronic absorption spectra of investigated porphyrins were recorded in phosphate-buffered saline (PBS). Due to the presence of four sulfonic groups (-SO_3H) all of the compounds are very well soluble in aqueous solutions and their spectra are typical of porphyrin derivatives confirming a lack of aggregation (Fig. 2). Table 1 illustrates the optical and photophysical properties of the porphyrin-based photosensitizers synthesized in this work as well as, commercially available, meso-tetra-(4-sulfonatophenyl)porphyrin (TPPS) as a reference compound. The introduction of fluorine atoms in the structure caused a slight blue shift of the Soret band, evident for the F_2POH absorption at 410 nm (Fig. 2a and Table 1). Upon metalation with Zn(II) and Pd(II), notable effects were observed in the π to π^* energy gap within the porphyrin electronic absorption spectra. PdF_2POH exhibited hypsochromic shifts due to the orbital mixing of the π orbital with the metal d_π orbital, forming a new low-energy electronic state. Conversely, coordination with Zn^{2+} led to a slight redshift in the Soret band (Fig. 2b), suggesting a weak π to d_π orbital interaction. Additionally, the spectra of the metalloporphyrins (PdF_2POH, ZnF_2POH) displayed a reduced number of Q bands compared to F_2POH. This reduction in number of Q bands is related the change in symmetry from D_{2h} to D_{4h}, explained by the Gouterman four-orbital model. As for the photophysical properties, ZnF_2POH is characterized by lower fluorescence quantum yield, shorter fluorescence lifetime and consequently higher rate of intersystem crossing to the triplet excite state than the corresponding free-base derivatives (Table 1 and Figure S1). No PdF_2POH fluorescence is observed within the 500–750 nm range (Fig. 2c). This effect can be attributed to the increased spin–orbit coupling originated from a heavy metal such as palladium [32]. A lower quantum yield of fluorescence should naturally result in a higher quantum yield of the triplet state and improved singlet oxygen generation. It is important to highlight that singlet oxygen plays a pivotal role in combating bacteria because there are no defense mechanisms against this species. Our results indicate that the examined photosensitizers can efficiently generate singlet oxygen, as they have sufficient energy for a direct transfer from their triplet excited state to molecular oxygen (Table S2). F_2POH generates singlet oxygen with a quantum yield of 0.78. This is higher than for TPPS, due to the presence of fluorine substituents in the phenyl rings. The incorporation of Zn^{2+} and Pd^{2+} ions had a significant effect on the formation of $^1O_2$. For ZnF_2POH, Φ_Δ reached

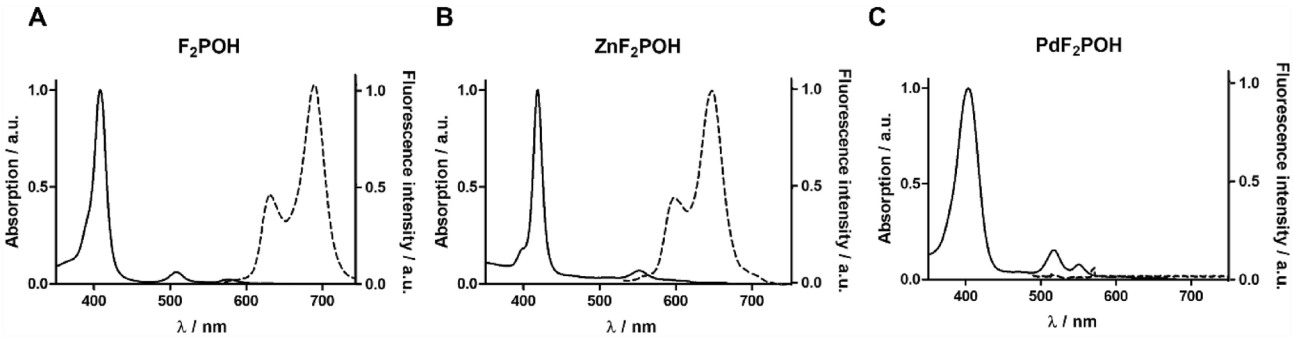

Fig. 2 Normalized electronic absorption and emission spectra of F_2POH, ZnF_2POH, PdF_2POH recorded in a phosphate-buffered saline (PBS) solution at room temperature

Table 1 The optical and photochemical characteristics of porphyrins determined in PBS at room temperature

	Absorption					Fluorescence		Triplet	Φ_Δ		logP
	B (0,0)	Q_y (0,1)	Q_y (0,0)	Q_x (0,1)	Q_x (0,0)	λ/nm	Φ_F	τ_{TAr}/μs	Direct	Indirect	
TPPS	414	546	512	590	648	649, 714	0.10[a]	2.2	0.64[a]	0.70	−1.2
F_2POH	412	505	540	585	641	645, 706	0.06	5.41	0.76[b]	0.78	−1.7
ZnF_2POH	423	–	–	554	592	600, 649	0.03	0.15	0.86[b]	0.83	−1.3
PdF_2POH	408	–	–	519	552	–	–	2.06	0.93	0.72	−1.2

[a]In DMSO [37]

[b][48]

0.86 (direct method), and there was a further increase for the palladium(II) complex ($\Phi_{\Delta} = 0.93$) (Figure S2, S3). This is explained by the heavy atom effect, which is more efficient for larger cations with complex electron structures, particularly those involving *d* orbitals [52]. As mentioned before, all of the porphyrins exhibit excellent water solubility (negative logP values) (Table 1).

2.3 Detection of ROS in solution

Photogenerated ROS can react with many biomolecules present in microbial cells. In addition to singlet oxygen, other ROS, such as hydroxyl radicals, superoxide ions, and hydrogen peroxide, also have crucial roles in augmenting oxidative stress boost during PDI [8, 53]. Thus, the ROS generation was also evaluated in porphyrin's PBS solution using fluorescent probes including SOSG (selective for singlet oxygen) [54], APF (overall oxidative stress), HPF (specific mostly to hydroxyl radicals), and DHE (specific for superoxide ions). Figure 3 demonstrates that the notable singlet oxygen quantum yields of the examined porphyrins were further verified through experiments involving the SOSG fluorescent probe (as illustrated in Fig. 3a). The effective generation of ROS was observed in the following order: $PdF_2POH > F_2POH > ZnF_2POH$ using APF (Fig. 3b).

Moreover, experiments conducted with the HPF probe, known for its higher specificity for hydroxyl radicals, indicate that PdF_2POH generates significantly higher amount of $HO^{\bullet}$than other porphyrins, as shown in Fig. 3c. The reduction of oxygen to superoxide ions ($O_2^{\bullet -}$) was tracked by their reaction with the DHE, which is a probe sensitive to superoxide ions and responsive in the presence of hydrogen peroxide (H_2O_2). The PdF_2POH indicates the highest DHE intensity compared to ZnF_2POH and F_2POH (Fig. 3d). The results obtained from these experiments provide confirmation that the introduction of metal ions amplifies the ability to generate ROS and allows for the fine-tuning of the underlying mechanisms. Interestingly, depending on the light doses used, both metalloporphyrins generate large amounts of singlet oxygen, but it is PdF_2POH that has the highest activity in generating ROS through both type I and type II photochemical mechanisms, especially compared to other fluorinated porphyrin derivatives.

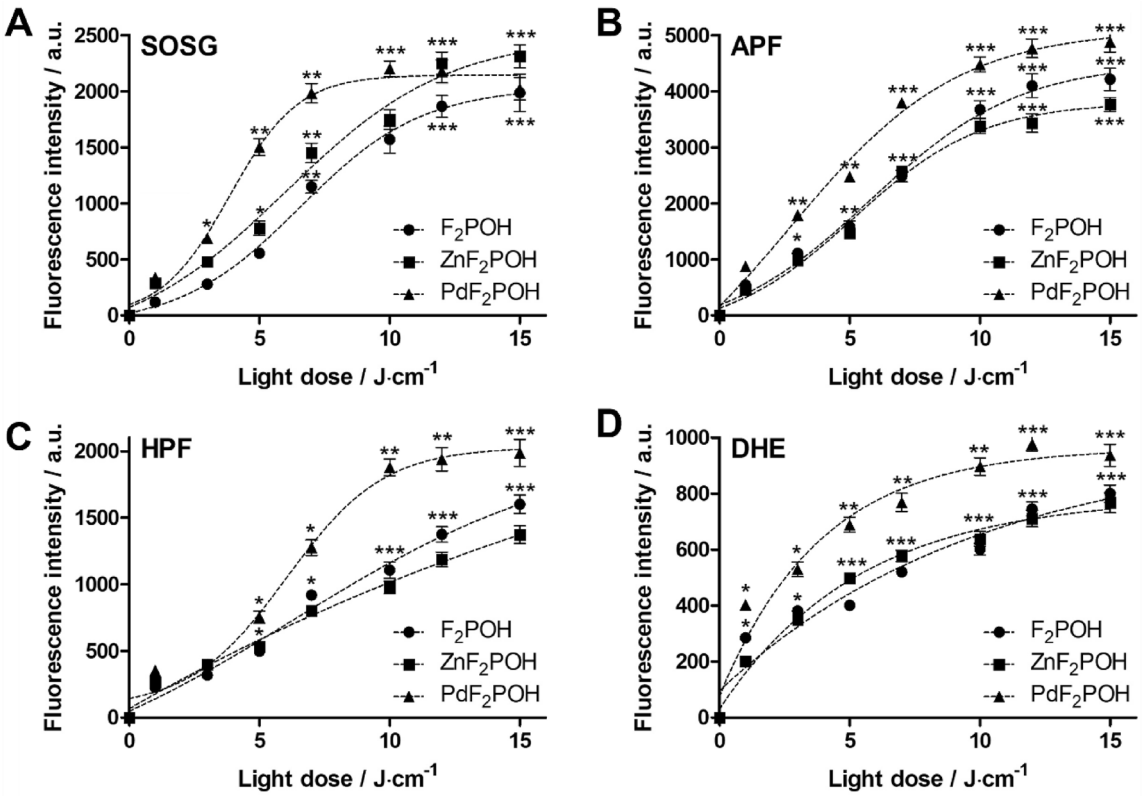

Fig. 3 ROS generation by porphyrins F_2POH, ZnF_2POH, and PdF_2POH determined in PBS using fluorescence probes: SOSG, APF, HPF, and DHE. The 20 µM solution of each porphyrin derivative prepared in PBS was mixed with a 50 µM solution of each probe, and the fluorescence intensity was measured for each porphyrin-probe pair during the irradiation with 420 ± 20 nm light: **a** SOSG, **b** APF, **c** HPF, and **d** DHE. Data are expressed as mean ± SEM ($n = 6$). The asterisks denote *p*-values $<^{*}0.05$; $^{**}0.01$; $^{***}0.001$ compared to control (Two-way ANOVA followed by Bonferroni multiple comparisons test)

2.4 Theoretical calculation

Quantum chemical calculations were employed to gain insights into the distribution of charge and preferred conformations of photosensitizers (Table S1–S2, Figure S4). The sulfonic group is a strong electron-withdrawing substituent, which means that it can pull electrons away from the adjacent atoms. This may increase the electron density of the porphyrin ring and make it more delocalized and polarized. This could potentially reduce the energy gap between the highest occupied molecular orbital (HOMO) and the lowest unoccupied molecular orbital (LUMO) of the porphyrin. As a result, this might improve its light absorption and charge transfer ability [37]. However, this effect may depend on whether the porphyrin has a metal ion in its center or not. In the absence of a metal ion, the central region within the porphyrin core, where a metal ion typically coordinates, displays a relatively high electron density, often rendering a blue region on the electron density map. This phenomenon is attributed to the presence of electron-rich nitrogen atoms in the pyrrole rings (Fig. 4a). However, with the introduction of eight electron-withdrawing fluorine atoms, the central region undergoes a shift towards an increased positive charge (Fig. 4b). Upon metalation, the metal ion at the porphyrin core receives electron density from the surrounding nitrogen atoms within the porphyrin rings (Fig. 4c and d). This results in the central region surrounding the metal ion taking on a red hue on the electron density map, indicating a decrease in electron density. Simultaneously, the surrounding porphyrin ligand becomes more electron-rich due to the electron density transferred to the metal ion. Notably, halogenated photosensitizers exhibit a higher charge density at the center of the ring compared to the corresponding non-halogenated and sulfonated analogue (TPPS), as anticipated. Meanwhile, derivatives containing metal ions in the structure exhibit a more negative charge on the exterior of the ring.

2.5 Bacterial uptake

In our previous work, we revealed that the accumulation of PS in bacterial cells is dependent on, i.e., molecular charge and functional group in the macrocycle structure [37, 55]. Figure 5. shows the bacterial uptake of porphyrins in Gram-negative (Fig. 5a and b) and Gram-positive species (Fig. 5c and d). These data indicated that derivatives bearing sulfonic acid substituents can bind to Gram-positive bacteria (*S. aureus*, *S. epidermidis*) efficiently. For Gram-negative species (*E. coli* and *P. aeruginosa*) the uptake is significantly diminished. Nevertheless, incorporation of the metal ion may facilitate a better attachment of even uptake by the bacterial cells, and in the case of ZnF_2POH and PdF_2POH the concentration of accumulated PS is higher than for

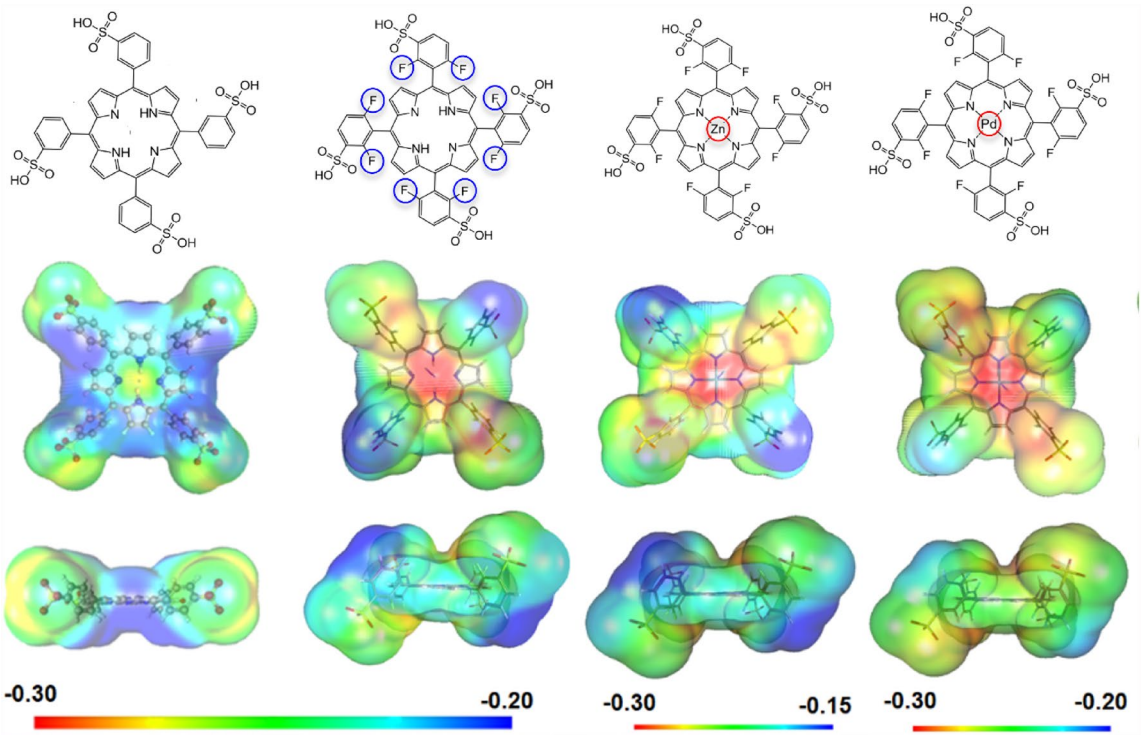

Fig. 4 The chemical structures of the studied photosensitizers and their electronic density maps created using the total self-consistent field density and were visualized with electrostatic potential. These maps are presented with an isovalue of 0.0004 in atomic units, and the calculations were carried out at the B3LYP/6-31G(d) level

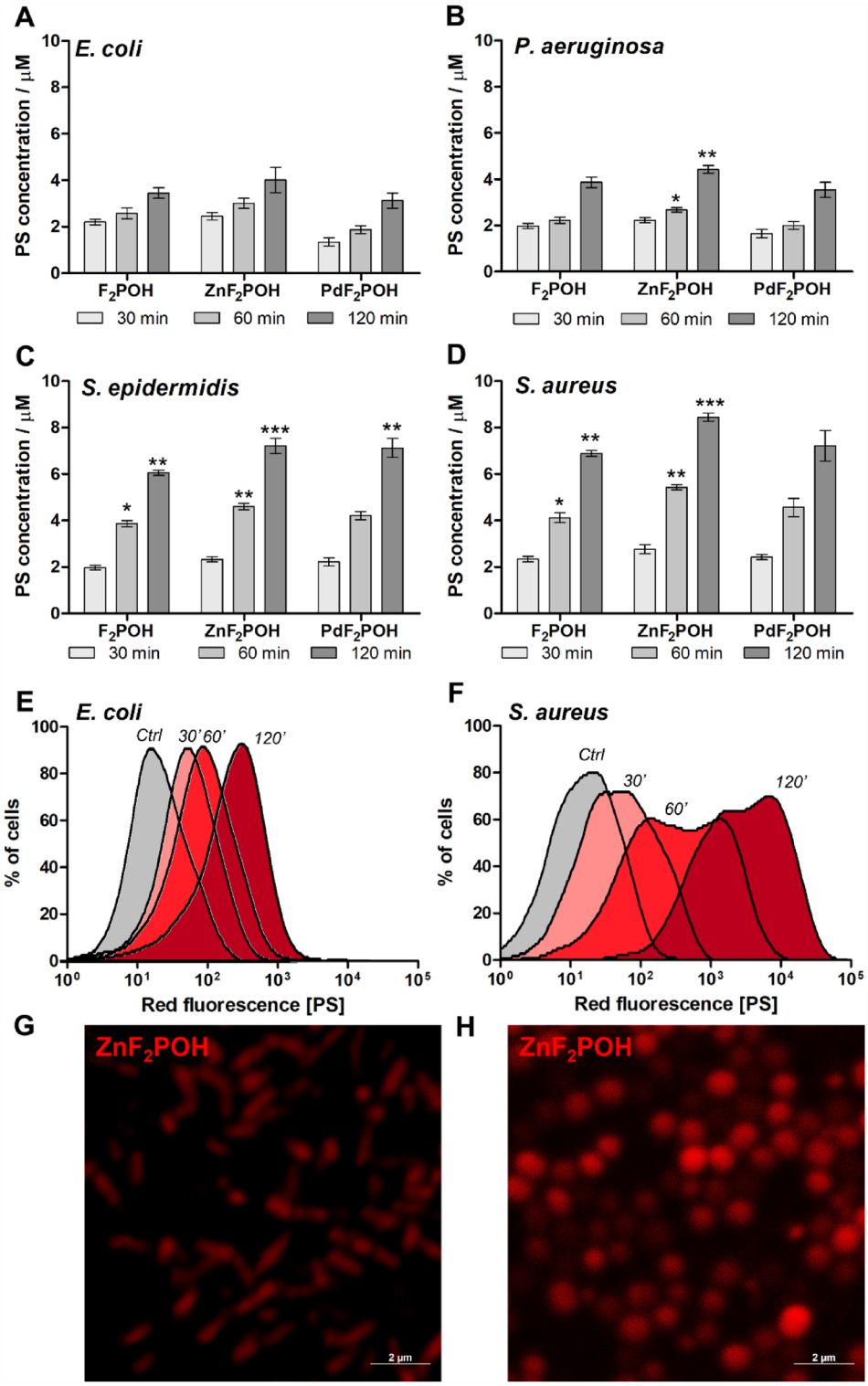

Fig. 5 Porphyrins accumulation in bacteria after 2 h incubation with 20 µM F_2POH, ZnF_2POH, and PdF_2POH in PBS. The porphyrin concentration in bacterial lysates was determined by absorption and fluorescence spectroscopy (**a**–**d**); the bacterial uptake of ZnF_2POH was also determined by flow cytometry (red fluorescence shift, **e** and **f**) and was visualized in confocal microscopy images using fluorescence properties of photosensitizer (*red signal*). Data are expressed as mean ± SEM ($n = 4$). The asterisks denote p-values $<^{*}0.05$; $^{**}0.01$; $^{***}0.001$ compared to sample after 30 min of incubation (Two-way ANOVA followed by Bonferroni multiple comparisons test) (color figure online)

F_2POH. This effect can be associated with the decreased susceptibility of Gram-negative bacteria to PDI, primarily because of the membrane barrier that hinders the uptake of anionic and neutral photosensitizers. The concentration of all studied photosensitizers in bacterial cells increases over time. The best cellular uptake was determined for ZnF_2POH. However, the uptake for PdF_2POH could be potentially even greater, but it is more difficult to determine it, because this derivative is not fluorescent, and the concentration was estimated by the absorption measurements in the lysates. The most significant accumulation was found in *S. aureus*. Based on recent reports, this may be related to the electrostatic

interaction with the membranes of Gram-positive bacteria, as well as to an "active transport" mechanism that represents a new pathway for metalloporphyrins in PDI [56]. One proposed hypothesis is that metalloporphyrins are recognized by heme transporters due to their similar structure to Fe^{3+}-protoporphyrin IX. Studies on the accumulation of metalloporphyrins showed that *S. aureus* cannot detoxify most of the toxic analogs through pump efflux in the same manner as heme [57]. Most of them accumulate in the *staphylococcal* cell membrane. Recent studies of PDI with Ga^{3+}PPIX showed rapid, diffusion-limited uptake of PS correlated with the appearance of cell-surface hemin receptors [58].

To conduct additional investigations into the cellular uptake, we proceeded to confirm the accumulation of ZnF_2POH using flow cytometry. Representative histograms registered for *E. coli* and *S. aureus* over time of incubation with PS are presented in Fig. 5e and f. Moreover, we also monitored the attachment/uptake of ZnF_2POH using confocal fluorescence microscopy (Fig. 5g and h). The data obtained from flow cytometry and fluorescence microscopy serve as complements to the uptake studies conducted using bacterial lysates. As expected, these results indicate a more substantial accumulation of the investigated photosensitizers in Gram-positive bacteria compared to Gram-negative ones.

2.6 Photodynamic inactivation of bacteria

The antimicrobial photodynamic activity of F_2POH, ZnF_2POH, and PdF_2POH was investigated against *E. coli*, *P. aeruginosa*, *S. aureus* and *S. epidermidis* in the planktonic culture at different light doses and PS concentration of 20 μM (Fig. 6). The chosen concentration did not result in any dark toxicity following a 2 h incubation period. Subsequently, the bacteria were exposed to 420 ± 20 nm light immediately after this incubation, without the need to wash out the porphyrin solution. This approach was undertaken because unbound PS molecules are also expected to be present in PDI clinical protocols, especially in applications targeting conditions such as skin infections. Based on our and other research groups' experience, PDI protocols involving short drug-to-light intervals (2 h in this work) [37, 47, 55] and relatively low light doses can effectively deactivate a wide range of pathogens.

The ability to employ shorter incubation times in PDI compared to the traditional anticancer photodynamic treatment stems from the rapid interaction between functional groups present in the PS structure and the components of the outer wall of bacterial and fungal cells. This characteristic plays a crucial role in determining the selectivity of antimicrobial cells concerning host eukaryotic cells, such as keratinocytes, particularly *in vivo*. Figure 6 shows the survival of these microorganisms after PDI. *E. coli* bacteria were less susceptible to PDI and only 1–1.5 log CFU was inactivated after PDT with ZnF_2POH and PdF_2POH and a light dose of 10 J/cm^2 (Fig. 6a). For *P. aeruginosa* the effect was slightly better and PDI with PdF_2POH at 10 J/cm^2 reached almost 3 logs of reduction as well as 2.3 logs and 2 logs for ZnF_2POH and F_2POH, respectively (Fig. 6b). The most significant PDI effect was determined for Gram-positive bacteria. For *S. aureus* 3 logs of reduction (99.9%) was observed after using PdF_2POH and 3 J/cm^2 light dose. Similar efficacy was found for ZnF_2POH. Once the light dose was increased to 5 J/cm^2, a biocidal effect was noted for all the photosensitizers tested (3.5 logs for F_2POH, 4 logs for ZnF_2POH and 4.2 logs for PdF_2POH). More importantly, for PdF_2POH-mediated PDI, almost complete inactivation (6 logs) of *S. aureus* was observed (Fig. 6c). Similarly, PDI proved to be just as effective against *S. epidermidis* (Fig. 6d). The fairly significant differences in the photodynamic inactivation of the Gram-positive and Gram-negative bacteria are largely attributed to structural differences in their cell envelopes. The improved photodynamic activity of PdF_2POH can be related to its high ability to generate ROS via both mechanisms (Type I and Type II). The activity of F_2POH is similar to our previously published data [21]. ZnF_2POH was previously used for the preparation of TiO_2-based hybrid materials [47, 48], but herein it is tested as a PDI photosensitizer in a homogeneous system for the first time. Overall, the final antimicrobial activity of the tested compounds is influenced both by the presence of a metal ion in the PS structure and by the high efficiency of generating various types of ROS (singlet oxygen and oxygen-centered radicals).

To further explore the PDI activity mediated by the investigated metalloporphyrins, we confirmed the presence of damaged cells by staining them after treatment with Calcein AM and propidium iodide (PI) (LIVE/DEAD staining) and imaging with confocal fluorescence microscopy. Figures 7 and 8 show the representative images of untreated and PDI-treated *P. aeruginosa* and *S. aureus*. The green fluorescence signal is characteristic for living cells labelled with Calcein AM. In contrast, the red signal from propidium iodide (PI) clearly indicated that after PDI, treated cells lost their integrity, allowing the dye (that is excluded by viable cells) to penetrate the cell membranes of disrupted or dead bacterial cells.

2.7 Detection of reactive oxygen species in bacterial cells

ROS photogenerated by investigated photosensitizers were also evaluated in situ in all four bacterial strains (Fig. 9). For this purpose, we use the Total Reactive Oxygen Species Assay to measure the ROS level in each time-point of irradiation, which during PDI action increases significantly, leading to oxidative stress and consequently, the destruction

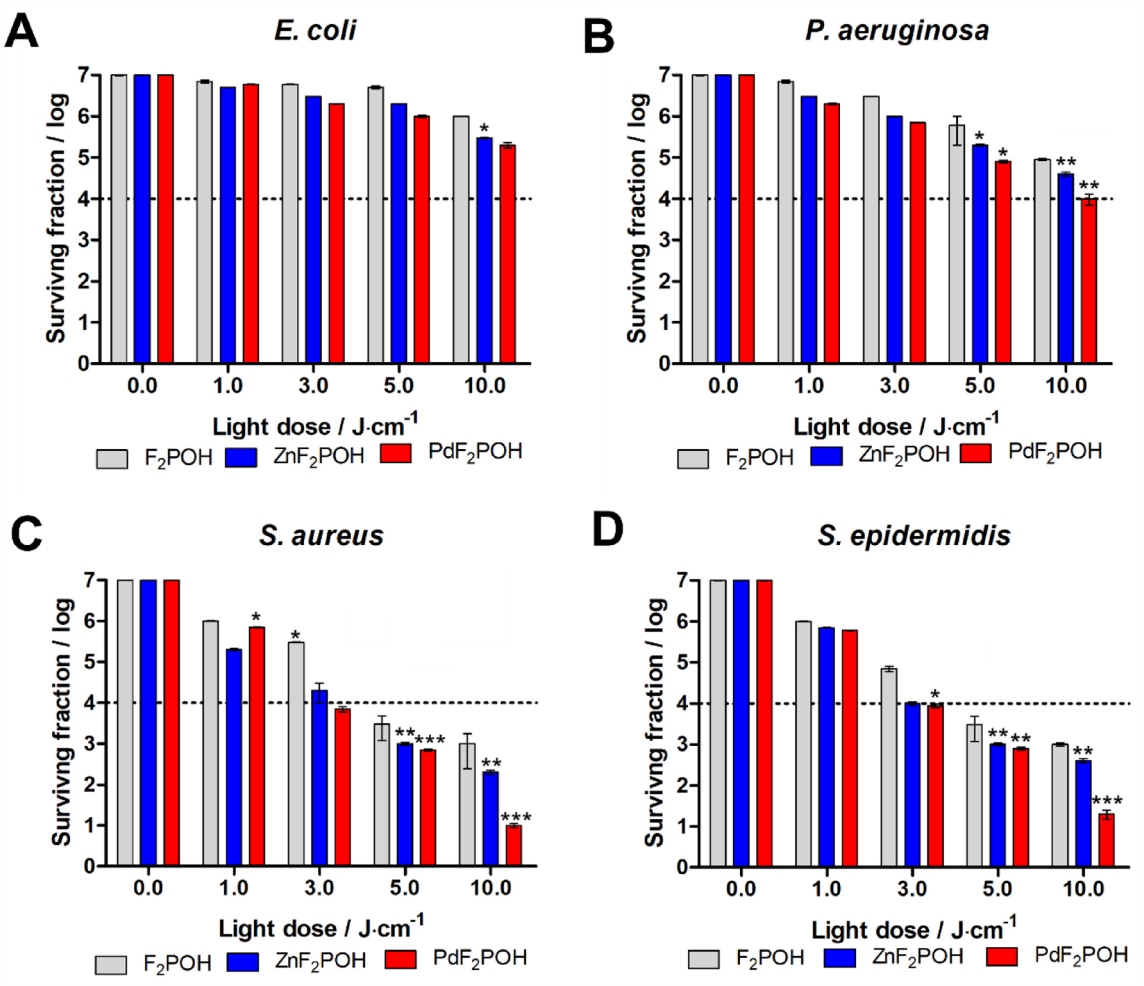

Fig. 6 Survival fractions of bacteria post-PDI with varying light doses, shown on a logarithmic scale. Panels **a** to **d** represent different bacterial strains: **a** *E. coli*, **b** *P. aeruginosa*, **c** *S. aureus*, and **d** *S. epidermidis*. The results are depicted for three distinct porphyrins: F_2POH (*grey*), ZnF_2POH (*blue*), and PdF_2POH (*red*). Each plot illustrates the impact of different light doses on bacterial survival. Bacteria were incubated with 20 µM PS aqueous solution in the dark and then irradiated with 420 ± 20 nm light. Data are expressed as mean ± SEM ($n = 6$). The *asterisks* denote *p*-values $<$ $^{*}0.05$; $^{**}0.01$; $^{***}0.001$ compared to control (Two-way ANOVA followed by Bonferroni multiple comparisons test) (color figure online)

of bacteria. Since bacterial cells contain intrinsic dyes and ROS, some fluorescence was also observed in the blank samples where no porphyrin was added. This signal was at various levels in each type of bacteria, which implies their different states of intrinsic defense systems against oxidative stress. After incubating the bacteria with porphyrins and a given fluorescent probe, a clear difference was observed compared to the blank sample in the increased presence of generated ROS inside the bacteria. In the case of *E. coli*, all three porphyrins generate a similar amount of ROS (Fig. 9a). However, increased levels of photogenerated ROS were observed in *P. aeruginosa*, *S. aureus* and *S. epidermidis* (Fig. 9b–d). The observed increase in ROS levels was greatest in bacteria treated with PdF_2POH, followed by ZnF_2POH and F_2POH. This data correlate well with the PDI experiments and confirm that generation of various types of ROS by photosensitizers plays a crucial role in bacteria deactivation. PdF_2POH turns out to be the most effective PS because it generates a higher amount of ROS according to both photochemical mechanisms.

2.8 Biofilm inactivation

S. aureus is a frequent causative agent of a wide spectrum of infections, spanning from superficial to potentially life-threatening. Moreover, bacteria in biofilms can be up to 1000 times more resistant to antibacterial agents than planktonic bacteria [59]. The PDI studies revealed that investigated porphyrins, especially Pd-derivative have superior potency in *S. aureus* photokilling. That is why we examined PSs efficacy

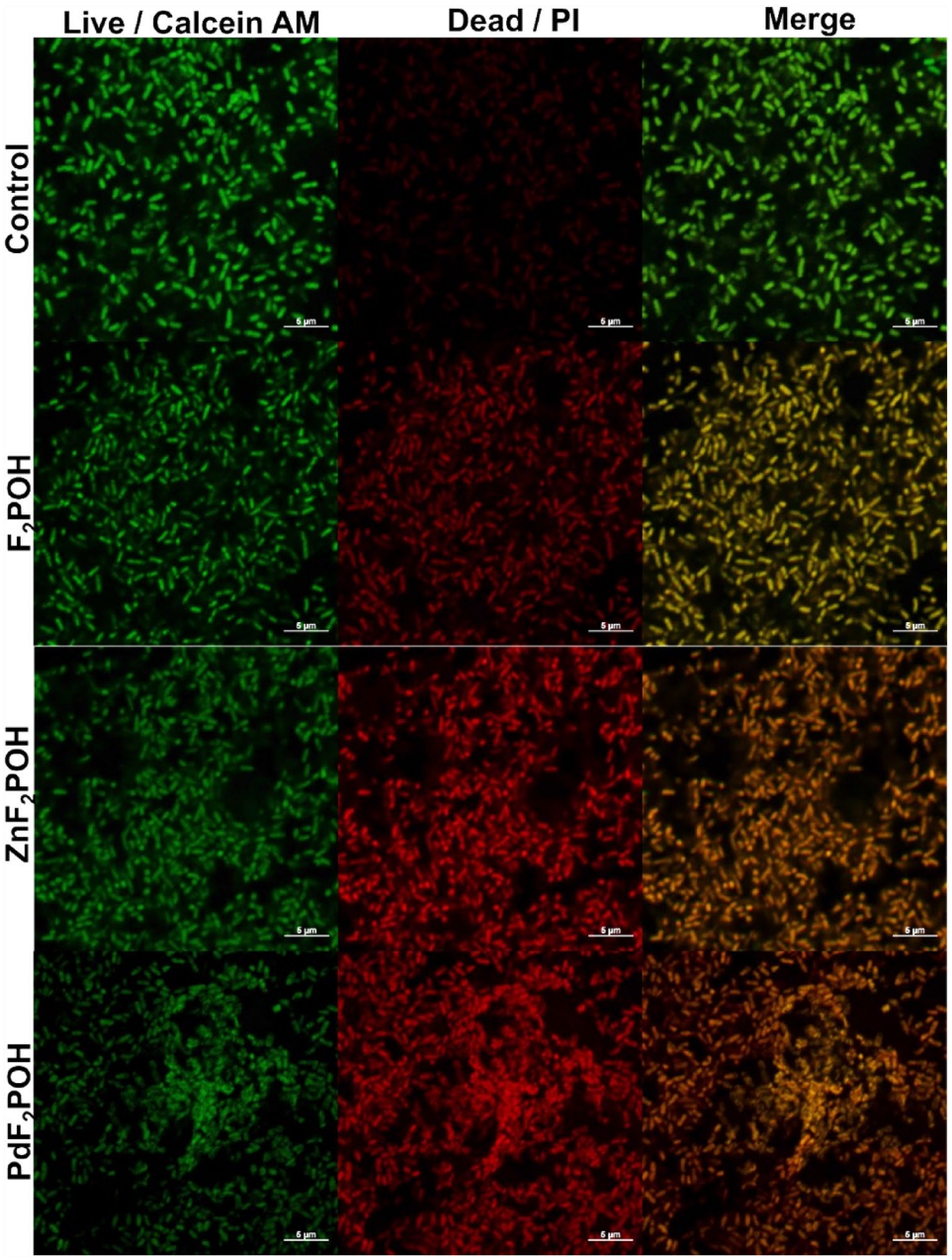

Fig. 7 Cell viability of *P. aeruginosa* after PDI treatment with investigated porphyrins (20 µM, 10 J/cm^2, 420 ± 20 nm light). The representative confocal microscopy images show the live (*green*) and dead (*red*) bacteria stained with Calcein AM and propidium iodide, respectively. The images are arranged in a matrix, where the rows correspond to the control and the three porphyrins (F_2POH, ZnF_2POH and PdF_2POH), and the columns correspond to the live, dead, and merged images. The scale bar is 5 µm (color figure online)

against *S. aureus* biofilms. Biofilms were obtained after incubation of the bacteria in 12-well flat-bottom sterile polystyrene microplates coated with an ultra-thin layer of agar for 24 h at 37 °C. Biofilms were cultured on a solid nutritive substrate that is exposed to air and only fed through the bottom substrate, which contains ions salts and nutrients for biofilm growth [60, 61]. Following the formation of the biofilms, they were subjected to a 2 h incubation with the photosensitizers (F_2POH, ZnF_2POH and PdF_2POH) at a concentration of 20 µM. Subsequently, the biofilms were exposed to 420 ± 20 nm light irradiation at 10 and 30 J/cm^2. Figure 10a shows the live/dead staining of prepared biofilms after PDI treatment. Based on the presented images, each porphyrin causes biofilm inactivation, but the most pronounced inactivation is observed for PdF_2POH. Control cultures showed no effect on biofilm. Moreover, the percentage of live and dead cells was estimated using color distribution quantification. These data indicated that F_2POH results in 25–35% of dead bacteria in biofilm, ZnF_2POH 40–50%, PdF_2POH 40% at 10 J/cm^2, and almost 70% of dead biofilm forms after PDI with 30 J/cm^2 (Fig. 10b).

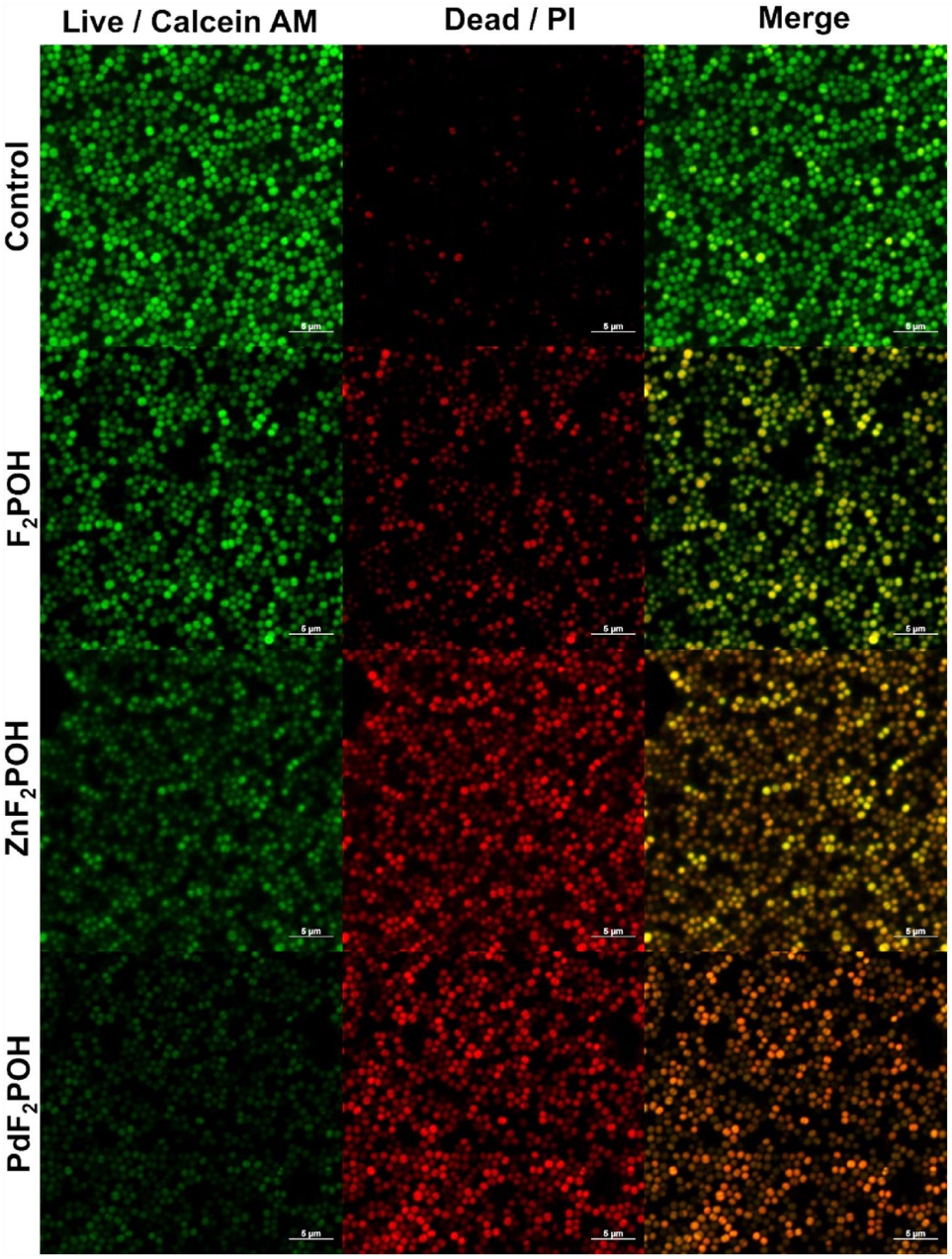

Fig. 8 Cell viability of *S. aureus* after PDI treatment with investigated porphyrins (20 µM, 10 J/cm^2, 420 ± 20 nm light). The representative confocal microscopy images show the live (*green*) and dead (*red*) bacteria stained with Calcein AM and propidium iodide (PI), respectively. The images are arranged in a matrix, where the rows correspond to the control and the three porphyrins (F_2POH, ZnF_2POH and PdF_2POH), and the columns correspond to the live, dead and merged images. The scale bar is 5 µm (color figure online)

2.9 Selectivity of porphyrin-derivatives towards human keratinocytes and inhibition the progress of S. aureus infection in vitro

The cytotoxicity and phototoxicity of the investigated photosensitizers were evaluated in human epidermal keratinocytes (HaCaT) cells. To estimate the possible selectivity over mammalian cells, the same experimental conditions as for PDI were applied. To determine the dark cytotoxicity induced by porphyrin derivatives, HaCaT cells were incubated with PS at a broad range of concentrations (0–100 µM) for 2 h, Fig. 11a. Cytotoxicity in the dark is negligible for almost all tested concentrations of the photosensitizers used. The viability of cells after using ca. 100 µM PS decreased to 90%. Photodynamic effect of tested porphyrins is depicted following a 2 h incubation of cells with a 20 µM of each PS and subsequent irradiation with light at 420 ± 20 nm over a range of 0–10 J/cm^2 (Fig. 11b). The onset of phototoxicity started with light doses higher than 7 J/cm^2. This data indicated that up to 5 J/cm^2 in applied experimental conditions the PDI procedure may be selective towards bacteria (PdF_2POH-PDI on *S. aureus* after using 3 J/cm^2 results in 99.9% of inactivation, as presented in Fig. 6c).

The low phototoxicity of F_2POH, ZnF_2POH, and PdF_2POH at short incubation times is readily understood considering that at early incubation times, ROS are

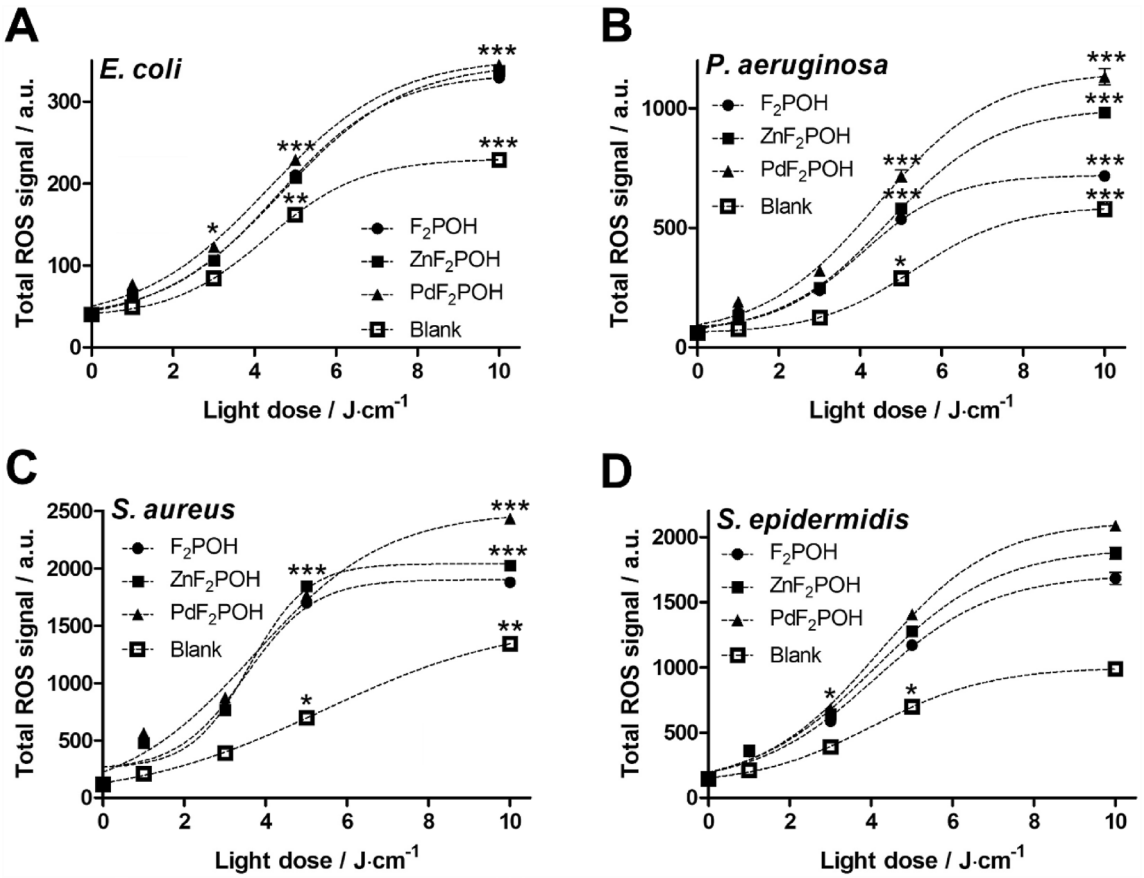

Fig. 9 Reactive oxygen species (ROS) generation in bacteria post-PDI for varying light doses. Panels **a** to **d** represent different bacterial strains: **a** *E. coli*, **b** *P. aeruginosa*, **c** *S. aureus*, and **d** *S. epidermidis*. The figure illustrates the ROS levels induced by three different porphyrins: F_2POH, ZnF_2POH, and PdF_2POH. Data are expressed as mean ± SEM ($n = 4$). The asterisks denote p-values $<^{*}0.05$ compared to control (Two-way ANOVA followed by Bonferroni multiple comparisons test)

generated outside the cell or in the cell membrane, and damage is essentially restricted to the cell membrane. Moreover, tested photosensitizers are characterized by negative logP values and possess a hydrophilic character. Thus, their accumulation in mammalian cells is reduced, in contrast to effective attachment to Gram-positive bacteria's membranes.

Invasion is also likely to play a key role, particularly in maintaining persistent or recurring microbial infections. In the next part of this work, we employed the well-characterized keratinocyte cell line HaCaT as an in vitro model to study the influence of porphyrin mediated PDI on bacterial invasion of the skin (Fig. 12). According to data published by Edwards et al. the invasion of *S. aureus* in HaCaT cells occurred more slowly than adhesion. After 15 min $<10^3$ CFU *S. aureus* was internalized, despite the high number of adherent bacteria, and there was no significant increase up to 30 min, indicating that the invasion process includes a lag-phase [62].

Thus, 15 min after starting the *S. aureus*-GFP infection (green fluorescence), we performed a low-light dose PDI (3 J/cm^2) with PdF_2POH to avoid the HaCaT cells (cytoskeleton—red fluorescence, nuclei—blue fluorescence) damage and utilize the appropriate selectivity of PDI over host cells with these experimental conditions. Then, we monitored the progress of the infection 30, 45, and 90 min after PDI compared to untreated *S. aureus*-infected HaCaT cells.

Obtained images showed that the applied PDI procedure can inhibit infection progress. In control cells, after 30 and 45 min from infection there are a lot of internalized bacteria that are located around the nuclei and, in the worst condition—fullfil the whole cells. By 90 min post-inoculation, in PDI untreated cells a number of fully internalized bacteria and completely "eaten" cells could be observed within the keratinocytes. In this case, *S. aureus* induces huge membrane alterations. Contrastingly, when PDI was applied, the infection progressed more slowly. After 30 and 45 min most of *S. aureus* bacteria accumulate around the nucleus, and after 90 min the infection starts to expand to the whole cytoplasm. Noteworthily, the cells are characterized by intact

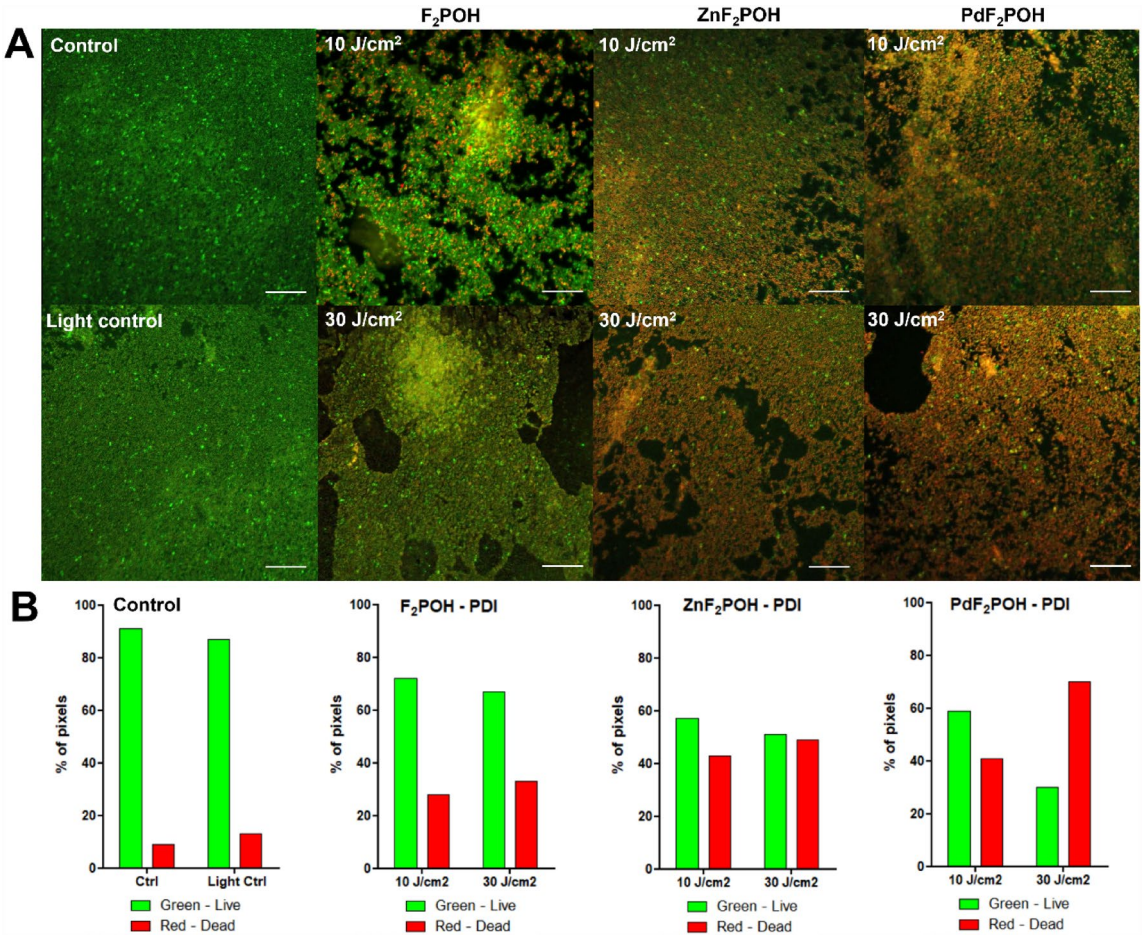

Fig. 10 **a** Representative confocal images of *S. aureus* biofilms: untreated control and treated with PDI mediated by F_2POH, ZnF_2POH, and PdF_2POH (20 μM, light doses of 10 and 30 J/cm^2). After PDI treatment, bacterial biofilms were stained with Calcein AM (live cells, green fluorescence) and propidium iodide PI (dead cells, red fluorescence). Scale bar is 20 μM. **b** *Green* and *red* signal intensity quantification that illustrates the proportion of live and dead cells in imaged biofilms. The quantification was performed using ImageJ Fiji software (color figure online)

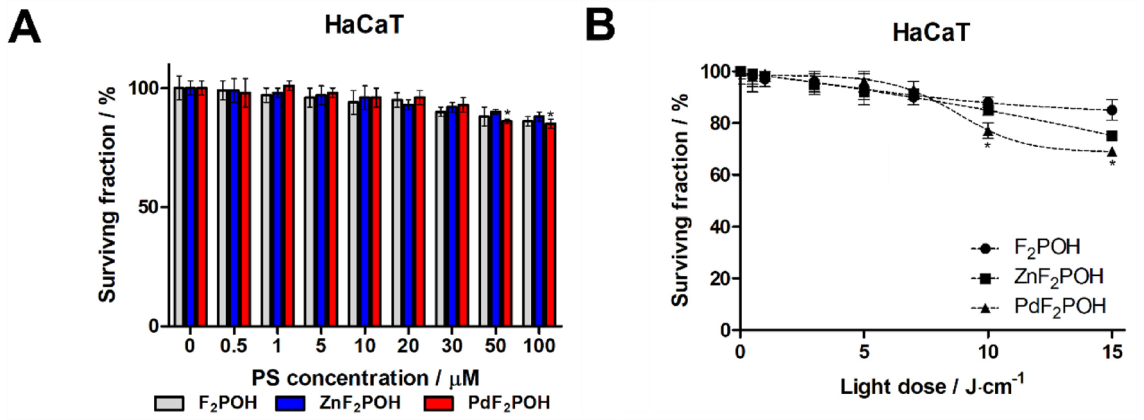

Fig. 11 Cytotoxicity and phototoxicity of different photosensitizers after a short incubation time. **a** Cell viability after incubation with 0–100 μM photosensitizers for 2 h without light irradiation. **b** Photodynamic effect mediated by 20 μM F_2POH, ZnF_2POH, and PdF_2POH and various doses of irradiation (0–15 J/cm^2) with 420 ± 20 nm light. Data are expressed as mean ± SEM (n = 6). The asterisks denote p-values $<^*0.05$compared to control (Two-way ANOVA followed by Bonferroni multiple comparisons test)

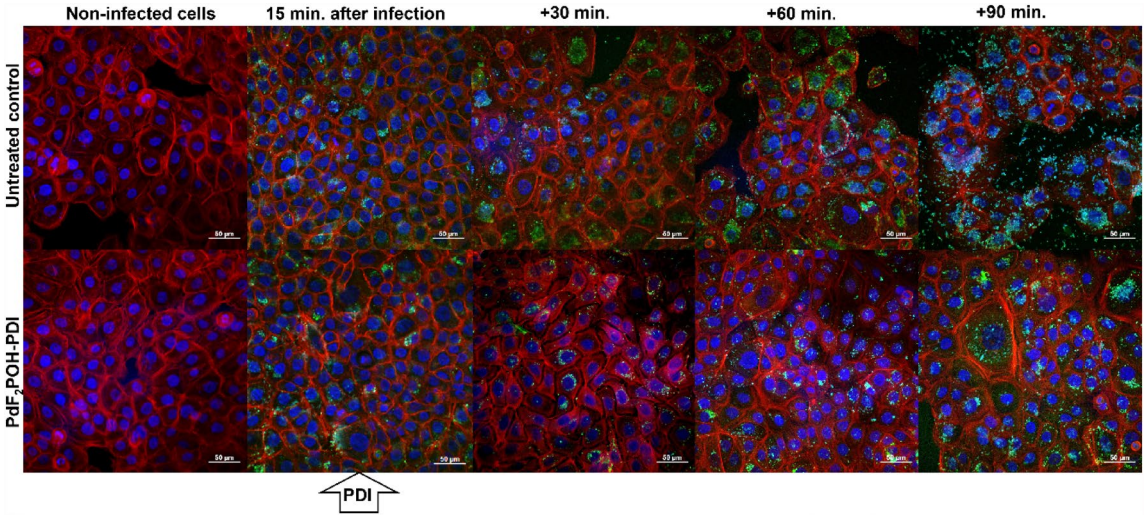

Fig. 12 The in vitro model of skin infection and the PdF_2POH-PDI impact of *S. aureus* invasion in HaCaT cells. Representative confocal pictures of HaCaT cells infected with *S. aureus*-GFP. HaCaT cells were co-cultured with *S. aureus*, then subjected to PDI and evaluated in the context of further bacteria invasion. After the end of experiment, HaCaT cells were fixed and stained with phalloidin and Hoechst33342 (cytoskeleton—red fluorescence; nuclei—blue fluorescence) and bacteria are characterized by green fluorescence. The images show the infection status in untreated (*upper*) and treated (*bottom*) cells at 15, 30, 60, and 90 min after infection and after PDI (color figure online)

membranes and a lower number of internalized bacteria than the control.

3 Discussion

The "One Health" approach has established its effectiveness in combating the microbial resistance pandemic comprehensively. This approach also underscores the importance of developing innovative strategies to combat pathogens [63]. While photodynamic therapy is primarily employed in cancer treatment, its potential for targeted microbial eradication offers numerous advantages over conventional antimicrobials and antibiotics. PDI boasts a wide spectrum of activity, capable of eliminating bacteria, fungi, and viruses [64]. Its antimicrobial action is immediate, in stark contrast to the hours or days often required by antibiotics [8]. PDI can effectively inactivate microorganisms, irrespective of their antimicrobial resistance profile, and its multifaceted mechanism significantly reduces the risk of selecting drug-resistant strains. These features make this photochemistry-based modality as an enticing avenue for exploration in the ongoing battle against infections [65]. PDI efficacy is closely related to the type of PS and depends on its chemical nature, properties as well as biological mechanisms in bacteria, such as efflux pumps [16, 37].

Structural modification of porphyrin derivatives through metalation or the introduction of peripheral substituents, represents a promising strategy aimed at obtaining molecules with the desired characteristics and practical uses [16, 66]. For example, the incorporation of sulfonic acid groups into the phenyl rings of porphyrins can enhance their water solubility, polarity, and negative charge, which may have significant implications for their antimicrobial activity. These sulfonic groups are easily deprotonated and may interact with the positively charged components of the bacterial membrane, such as lipopolysaccharides, lipoproteins, and phospholipids, and cause membrane permeabilization and leakage of cytoplasmic contents. This may lead to cell death or increased susceptibility to other antimicrobial agents [67–69]. Palladium porphyrins have recently gained significant attention in photodynamic research, primarily due to their exceptional capacity to generate ROS through both Type I and Type II mechanisms. In a study conducted by Mroz et al., an investigation into the photophysical properties of a series of water-soluble porphyrins with imidazolium substituents was carried out. These porphyrins featured central metal ions such as Zn^{2+}, Pd^{2+}, and In^{3+}. The study aimed to elucidate the influence of the central metal ion on both the photophysical characteristics and the photodynamic effectiveness of these imidazolium-substituted porphyrins. The palladium porphyrin exhibited the highest triplet excited state quantum yield (≥0.99) compared to zinc (~0.9) and indium porphyrins, which correlated with its enhanced ROS generation and PDT efficacy in vitro [30, 31]. The same trend in efficacy with metal ions (e.g., $Pd^{2+} > Zn^{2+}$) was also reported for dicyanobacteriochlorins. Once more, the Pd-containing PS demonstrated the highest phototoxicity against cancer cells and exhibited the most efficient generation of hydroxyl radicals [70]. In 2019, Hamblin and

co-workers investigated the antimicrobial activity of two amphiphilic tetracationic porphyrins (FS111 and FS111-Pd). The palladium porphyrin exhibited higher activity compared to the free-base compound. PDI with a light dose of 10 J/cm^2 and PS at a concentration of 10 nM resulted in the complete eradication (achieving more than a 6-log reduction in viability) of MRSA. In the case of *E. coli* as well as *C. albicans*, the palladium complex displayed slightly greater activity than the free-base compound [32]. Lazerri et al. reported amphiphilic Pd(II)-porphyrin bearing trifluoromethyl group as a promising photosensitizer for PDI. They found that tricationic Pd(II)-porphyrin is able to cause up to a 5.5 log (99.999%) reduction of *E. coli* (10 μM, 5 min irradiation with visible light) [71]. A series of porphyrin-based photosensitizers with porphyrin conjugates linked via an alkyl chain (Monopor, Dipor, and Tripor) with chelated Pd(II) was described as promising photodynamic agents. As expected, the palladium complexes showed higher ROS generation (compared to free-base analogues) [29]. Pd(II) and Zn(II) complexes are also attractive in phthalocyanine-based photosensitizers [72]. For instance, Sobotta et al. described Zn(II)- and Pd(II)-phthalocyanines that revealed high quantum yields of singlet oxygen generation (0.55–0.77). Moreover, a clear relationship was observed between the presence of zinc(II) or palladium(II) ions in the core of the macrocycles and their photocytotoxicities against antibiotic-resistance pathogens (MRSA, *E. coli* (ESBL+), *C. albicans* resistant to fluconazole and *C. auris*). Palladium phthalocyanine derivative was noticeably more bactericidal against all tested microorganisms, including up to ~3.5 log reduction of *C. auris* [73].

In this context, we evaluated halogenated and sulfonated porphyrins containing Zn(II) and Pd(II) as photosensitizers for PDI, both in suspended culture and within biofilms. These porphyrins have been designed to enhance ROS generation, which is one of the most crucial factor for the PDI efficacy. We have shown that studied porphyrins, especially PdF_2POH, can reduce the surviving fraction of Gram-negative *P. aeruginosa* by 3 logs of killing and Gram-positive bacteria—*S. epidermidis* and *S. aureus* by 6 logs units at 20 μM concentration and 10 J/cm^2 irradiation of 420 ± 20 nm light. Multiple mechanisms contribute to the resistance of bacterial biofilms, including reduced diffusion of antimicrobials, deactivation of drugs by outer biofilm layers, and bacterial dormancy in certain biofilm regions [74]. We indicated that the investigated porphyrin derivatives (F_2POH, ZnF_2POH, PdF_2POH) are able to inactivate bacterial biofilm, but Pd(II)-porphyrin exhibited the highest efficacy, causing a higher number of dead cells after PDI. These findings provide that PdF_2POH, due to the high yield of ROS generation, may be used for treating bacterial infections associated with biofilms pose greater challenges for elimination. Moreover, for further determination of PDI efficacy, we applied the in vitro infection model of *S. aureus* invasion in human keratinocytes (HaCaT cells). The effect of PDI on bacterial invasion may be an interesting alternative because the poor penetration of many antibiotics into mammalian cells means that intracellular *S. aureus* could represent a reservoir for persistent infection. Thus, our data strongly suggest that PdF_2POH-PDI could be effective at reducing *S. aureus* invasion and inhibiting the fast progress of infection and, consequently, healthy cell destruction. Such an approach may have the added benefit of preventing invasion by other skin-colonizing pathogens. Our results suggest that Zn(II) and Pd(II) fluorinated porphyrins offer new opportunities for PDI of antibiotic-resistant bacteria and biofilms, which are major challenges for public health.

4 Conclusions

The "One Health" strategy effectively tackles the microbial resistance pandemic, highlighting the potential of PDI for targeted microbial eradication. Metalloporphyrins studied in this work, notably PdF_2POH, demonstrate superior efficacy due to their exceptional ROS generation capabilities. In experiments against *P. aeruginosa*, *S. epidermidis*, and *S. aureus*, PdF_2POH-PDI significantly reduced bacterial viability, particularly in challenging biofilm environments. This promising porphyrin also displayed potential for reducing *S. aureus* invasion in a human keratinocyte model, suggesting effectiveness against persistent infections. The study underscores the value of PdF_2POH-PDI in inhibiting infection progression and preventing invasion by skin-colonizing pathogens. Overall, Zn(II) and Pd(II) fluorinated porphyrin complexes, with PdF_2POH as a notable candidate, present new opportunities for photodynamic inactivation of antibiotic-resistant bacteria in planctonic and biofilm forms. The multifaceted approach involving ROS generation and targeted microbial eradication positions PdF_2POH as a promising avenue in the ongoing battle against infections, offering potential solutions to combat antibiotic resistance and address biofilm-associated challenges in public health.

5 Materials and methods

5.1 Synthesis of metalloporphyrins

Synthesis of 5,10,15,20-tetrakis(2,6-difluoro-3-sulfonylphenyl)-palladium(II) pophyrin: 50 mg of 5,10,15,20-tetrakis(2,6-difluoro-3-sulfonylphenyl)-pophyrin (0.043 mmol) was dissolved in 10 mL of anhydrous DCM, then anhydrous palladium(II) acetate (48 mg, 0.215 mmol) was added. The whole was stirred in an atmosphere of inert gas (argon) at a temperature of 40 °C in the absence of light.

The reaction was monitored by electronic absorption spectroscopy, the end of the reaction was the transformation of four Q bands into two. After approximately 48 h, the mixture was rinsed with water and a saturated NaCl solution. The collected organic fraction was dried over anhydrous $MgSO_4$ and the solvent was evaporated. The product was obtained with a yield of 86%. Hydrolysis was then carried out (12 h, 120 °C). ^{1}H NMR (300 MHz, DMSO-d6) 8.88 (s, 8H, β-H); 8.22 (m, 4H, Ph-H); 7.54 (m, 4H, Ph-H), elemental analysis (%) for $C_{44}H_{20}F_8N_4O_{12}PdS_4$: C 44.66, H 1.70, F 12.84, N 4.73, O 16.22, S 10.84, Pd 8.99; exp: C 46.42, H 1.85, N 4.93, S 11.08.

Synthesis of 5,10,15,20-tetrakis(2,6-difluoro-3-sulfonylphenyl)-zinc(II) pophyrin: 50 mg of 5,10,15,20-tetrakis(2,6-difluoro-3-sulfonylphenyl)-pophyrin (0.043 mmol) was dissolved in 10 mL of anhydrous DCM, then anhydrous zinc(II) acetate (39 mg, 0.215 mmol) in anhydrous methanol was added. The whole was stirred under an inert gas atmosphere (argon) at room temperature. The reaction was monitored by UV–Vis spectroscopy, the end of the reaction was the transformation of four Q bands into two. After this time, the mixture was rinsed with water and a saturated NaCl solution. The collected organic fraction was dried over anhydrous $MgSO_4$ and the solvent was evaporated. The product was obtained with a yield of 90%. Hydrolysis was then carried out. ^{1}H NMR (300 MHz, DMSO-d6) 8.77 (s, 8H, β-H); 8.19 (m, 4H, Ph-H); 7.47 (m, 4H, Ph-H), elemental analysis (%) for $C_{44}H_{20}F_8N_4O_{12}S_4Zn$: C 46.26, H 1.76, F 13.31, N 4.90, O 16.81, S 11.23, Zn 5.72; exp: C 46.42, H 1.85, N 4.93, S 11.08.

5.2 Optical, photophysical and physicochemical properties of photosensitizers

Electronic absorption spectra measurements: The porphyrin-derivatives (F_2POH, ZnF_2POH, PdF_2POH) were dissolved in PBS. Electronic absorption spectra were acquired using quartz cuvettes with a path length of 1 cm. The spectra were recorded using UV-3600 Shimadzu spectrophotometer in the wavelength range of 350–700 nm.

Fluorescence measurements: Fluorescence spectra of F_2POH, ZnF_2POH, PdF_2POH were obtained within the wavelength range of 500–750 nm, with excitation at the Soret band of each porphyrin derivative. These measurements were conducted using a FluoroLog-3 Spectrophotometer. The samples were prepared in the following manner: initially, they were adjusted to an absorbance intensity at the Soret equal to 0.2. Subsequently, the samples were diluted by a factor of 100 for fluorescence measurement.

Triplet state lifetimes: The lifetime of the triplet excited state was determined using an Applied Photophysics LKS 60 laser flash photolysis spectrometer, which was equipped with a Hewlett-Packard Infinitum Oscilloscope. The excitation source employed for this purpose was the Spectra-Physics Quanta-Ray GCR-130 Nd: YAG laser. Samples were irradiated with the third harmonic of the laser at 355 nm (E_{max} = 100 mJ/pulse, FWHM = 6 ns). At least five kinetic decays were registered for each condition and the values were averaged. All solutions were prepared with absorbance around 0.2 at 355 nm. Experiments were made with solutions saturated in air and argon, for the measurements without oxygen. Purging with argon was made in a cuvette with septum for ca. 10 min for each sample, immediately before measuring. Absorption decays were collected at 460 nm and fitted to single exponential models.

Singlet oxygen quantum yield: The singlet oxygen quantum yield was determined by two different methods (direct and indirect). The first one ascertained by monitoring the phosphorescence at 1270 nm under ambient room temperature conditions. Singlet Oxygen Detection with DMA—indirect method: DMA (9,10-dimethyloanthracene) serves as a specific probe that undergoes a reaction with singlet oxygen, ultimately forming an endoperoxide. This reaction facilitates the identification and quantification of Φ_Δ. The solutions of F_2POH, ZnF_2POH and PdF_2POH with addition of DMA were prepared and subjected to irradiation using a 420 ± 20 nm LED diode. The decrease in the DMA absorption spectra at 377 nm during irradiation with F_2POH, ZnF_2POH and PdF_2POH confirmed the production of singlet oxygen. In contrast, a control sample (DMA only) was concurrently observed and showed no DMA photodegradation without the porphyrin derivatives.

ROS detection with fluorescent probes: To detect specific reactive oxygen species, various fluorescent probes were utilized. Hydroxyphenyl fluorescein (HPF) was employed to selectively detect hydroxyl radicals; Singlet Oxygen Sensor Green® (SOSG) for singlet oxygen; APF for both singlet oxygen and radical species, and dihydroethidium (DHE) for superoxide ion detection. These fluorescent probes at 50 μM were added to the solution of F_2POH, ZnF_2POH and PdF_2POH prepared in microplate wells at concentration of 20 μM. The PS solutions were then exposed to LED light at 420 ± 20 nm for varying durations. A microplate reader, the Tecan Infinite M200, was utilized for assessing the fluorescence intensity signal both prior to and subsequent to the light exposure, following the suitable excitation and emission parameters (accordingly to the probe manufacturer's protocols).

LogP determination: The partition coefficient (logP) of F_2POH, ZnF_2POH and PdF_2POH was assessed using the shake-flask method. To account for the partial solubility of solvents in one another, a small quantity of each porphyrin was dissolved in n-octanol-saturated PBS. The sample was then sonicated until complete dissolution of porphyrin. Subsequently, an equal volume of n-octanol-saturated PBS was added, and the experiment proceeded as

previously described. The resulting mixture was vigorously mixed using vortex and the photosensitizer's solutions were subjected to centrifugation to ensure precise phase separation. Next, 0.02 mL from each phase was extracted and diluted in 3.98 mL of DMSO. This was followed by a 5-min sonication of obtained dilution of F_2POH, ZnF_2POH and PdF_2POH and the measurement of fluorescence/absorption spectra were measured. A calibration curve was established to determine the concentration of F_2POH, ZnF_2POH and PdF_2POH in prepared solutions. The curve was constructed using the fluorescence or absorbance (for Pd-derivative) of the compounds in a serial dilution in DMSO with a 0.5% PBS buffer/n-octanol over a concentration range 1–100 nM.

5.3 Theoretical calculations

The optimization of molecular structures of TPPS (reference compound), F_2POH, ZnF_2POH and PdF_2POH was achieved through the density functional theory (DFT) method, utilizing the B3LYP hybrid functional and the 6-31G(d,p) basis set. Calculations encompassing geometry, highest occupied molecular orbital (HOMO), lowest unoccupied molecular orbital (LUMO), and electron density maps were executed with the Gaussian 9 software package. To consider solvent effects, specifically with a dielectric constant $\varepsilon = 78.54$ corresponding to water, solvent environment functionals were applied alongside the polarizable continuum model (PCM). The visualization of molecular structures of photosensitizers and orbital contour plots was carried out using the Gabedit software.

5.4 Antimicrobial activity of porphyrin derivatives

Bacterial strains and culture conditions: The study encompassed the utilization of Gram-positive bacteria, including *S. aureus* and *S. epidermidis*, as well as a Gram-negative bacteria: *E. coli*, and *P. aeruginosa*. *S. aureus* (NTCT 8325-4) and *S. aureus-GFP* were cultivated in brain heart infusion (BHI) medium, whereas *E. coli* (K12 ATCC10798), *S. epidermidis* (ATCC12228), and *P. aeruginosa* (ATCC19660) were cultured in LB broth. *S. aureus* were obtained with pTH2/pTH2-GFP plasmid that contains chloramphenicol resistance. These bacterial cultures were maintained at 37 °C with aeration, achieved by agitating them at 180 rpm. The growth of these bacterial cultures was tracked by measuring the absorbance at 600 nm (OD_{600} values) until it reached a value of 0.5—which corresponded to an estimated concentration of approximately 10^7 colony-forming units per milliliter (CFU/mL).

Photosensitizer binding to microorganisms—attachment/uptake investigations: The microorganisms were incubated with F_2POH, ZnF_2POH and PdF_2POH (20 μM) for specified time intervals (0–120 min.), in the dark at room temperature. Any excess, unbound photosensitizer was removed through two rinses using Ca^{2+} and Mg^{2+}-free PBS. Following the second rinse, the bacterial cells were lysed in a 10% SDS solution for a duration of 24 h. The degree of each photosensitizer uptake (F_2POH, ZnF_2POH and PdF_2POH) by the bacterial cells was assessed by measuring fluorescence or absorption (for PdF_2POH) spectra in each sample of lysate using a microplate reader (Tecan Infinite M200Pro). Uptake values were determined by estimating the photosensitizer concentration in lysates. The cellular attachment/uptake of the photosensitizers—F_2POH, ZnF_2POH and PdF_2POH was also evaluated with flow cytometry, quantifying it based on the red fluorescence of porphyrins. To perform this analysis, bacteria cells were incubated with porphyrin-derivative at a concentration of 20 μM for 2 h in PBS. Subsequently, the cells underwent two washes with HBSS and were prepared for analysis. The bacteria were then centrifuged and resuspended in 100 μL of PBS and examined using a Guava® easyCyte™ flow cytometer. The acquired data were processed with InCyte software (MerckMillipore, Burlington, MA, USA) dedicated to this equipment. The uptake of ZnF_2POH was additionally validated through confocal imaging, employing a Zeiss LSM880 with oil 100× objective. In the uptake studies, the bacteria were similarly exposed to the ZnF_2POH (20 μM) for 2 h. After washing, the bacterial samples were placed on glass slides for microscopic imaging. The captured images were analyzed utilizing Zeiss ZEN software.

Photoinactivation of microorganisms: The tested microorganisms (*E. coli*, *P. aeruginosa*, *S. aureus* and *S. epidermidis*) were treated with a 20 μM solution of F_2POH, ZnF_2POH, PdF_2POH in PBS for 2 h in dark environment at room temperature. Subsequently, aliquots of these cultures were transferred to a 12-well plate and irradiated with different doses of 420 ± 20 nm light, ranging from 0 to 10 J/cm^2. Following the light exposure (or, for the control group, incubation in darkness), the samples of treated bacteria were mixed, serially diluted in PBS, and then plated on LB agar to quantify the CFUs. Microorganism survival fractions were additionally assessed using the LIVE/DEAD BacLight Bacterial Viability Kit (Invitrogen).

ROS detection in bacterial cells: To determine the ROS level in vitro the Total Reactive Oxygen Species Assay Kit was used according to the protocol. Briefly, the bacteria cells were incubated with PS (20 μM) for 2 h in the dark and then the ROS Assay Stain stock solution was added for 1 h in the incubator. Subsequently, the bacteria were exposed to irradiation with 420 ± 20 nm light with various doses to stimulate the generation of ROS. A microplate reader (Tecan Infinite M200 Reader) was applied to detect the increase in fluorescence intensity before and after irradiation with the excitation/emission 488/520 nm.

Fluorescence confocal imaging of bacteria: The assessment of live/dead cells was conducted through fluorescence imaging using a confocal Zeiss LSM88 microscope. Bacteria were exposed to the photosensitizer solution at a concentration of 20 μM for a duration of 2 h. Following a thorough rinsing, the bacterial samples were treated with propidium iodide (PI) at 10 μg/mL and Calcein AM at 1 μg/mL. After another round of washing with PBS, these bacterial samples were positioned on glass slides for imaging using confocal microscope. The captured images were subsequently analyzed utilizing Zeiss ZEN software.

Biofilm formation: To prepare the *S. aureus* colonies that had been grown on suitable agar overnight, they were suspended in a growth medium, and the optical density at 490 nm (OD_{490}) was adjusted to 0.65. The resulting bacterial suspension was then diluted 1:6, which involved mixing 1 mL of the bacterial suspension with 5 mL of pre-warmed medium. The diluted suspension was then placed in an incubator at 37 °C with 5% CO_2 for roughly 3 h to reach the mid-logarithmic growth phase. Afterward, the mid-log growth suspension was additionally thinned at a ratio of 1:2500 using pre-warmed medium, and 200 μL of this diluted mixture was introduced into each well of an 8-well chamber slide coated with a thin layer of agar. After approximately 16 h, the medium from each chamber was aspirated and replaced with fresh medium. The biofilm was then exposed to specific composite materials for 24 h and subsequently visualized using fluorescence microscopy.

Biofilm visualization: To visualize the biofilm after the PDI, the following steps were carried out: the medium from each chamber was carefully removed, and the biofilm was washed twice gently with sterile saline. Next, the staining dyes (BacLight Live/Dead), were added into each well and allowed to incubate at room temperature for 15 min. During this incubation period, the samples were shielded from light. After the incubation, the staining solution was aspirated, and the biofilm was washed again with sterile saline, as performed previously. In the following phase, formalin (3.7% PFA) was introduced into each well, and the samples were left at room temperature for 30 min to fix the biofilms. The biofilm was washed twice with saline, and the wash fluids containing formalin were discarded. A mounting medium was applied, and a coverslip was placed on top of the sample. The biofilms were visualized using a Zeiss880 confocal microscope, and the images obtained were subsequently analyzed using Zeiss ZEN software.

Invasion model and PDI: The adhesion/invasion model of infection was developed. HaCaT cells were infected with bacterial suspensions containing either 1×10^7 CFU of *S. aureus*-GFP, diluted in fresh culture medium (DMEM + 5% FBS) to a final volume of 1000 μL and added to confluent monolayers of HaCaT. After 15 min of incubation (37 °C, 5% CO_2), the media were removed, and the cell monolayers were rinsed twice with PBS to wash out the planktonic bacteria, thus leaving the cell-adherent bacteria and the bacteria that had already invaded the cells. 20 μM solution of PdF_2POH was added to the wells with infected cells. The cells were incubated in the dark for a duration of 15 min. Then, the infected cells were irradiated with 420 nm light at a total dose of 3 J/cm^2. In the subsequent stage, the cells were rinsed with PBS to eliminate the photosensitizer solution, after which fresh medium was added. The progress of infection was monitored at 30, 45, and 90 min after PDI. At each time point, the cells were washed, fixed with 3.7% PFA and stained with falloidin-ATTO565 and Hoechst33342. Then cells were imaged using fluorescence confocal microscopy Zeiss 880.

5.5 Statistical analysis

The data are expressed as mean ± standard error of the mean (SEM), with 'n' representing the number of experiments conducted. Each experiment was replicated 4–6 times. Statistical analysis was performed using GraphPad Prism version 5.0.0 for Windows, GraphPad Software (San Diego, California, USA), employing two-way ANOVA with Bonferroni post hoc test. Significant distinctions between groups were assessed at p-values < 0.05, 0.01, and 0.001, denoted by *; **; and ***, respectively.

Supplementary Information The online version contains supplementary material available at https://doi.org/10.1007/s43630-024-00538-1.

Acknowledgements The work was the result of the implementation of the research project (Sonata Bis) number 2016/22/E/NZ7/00420 given to JMD funded by the National Science Center (NCN), Poland. Some of the research tasks (e. g., theoretical calculations) were supported by NCN grant no 2016/22/E/NZ7/00420. This research was possible due to the the support of PLGrid infrastructure grant plgsano4-cpu on the Ares supercomputer cluster.

Author contributions MW performed synthesis, compounds purification, and analysis. AS performed the calculations. MW, JMD and AS performed photophysical studies. BP and AB performed biological studies. BP and JMD conceived the studies and wrote the manuscript. JMD supervised the study, administered the project, and acquired funding. All authors revised the manuscript.

Funding Narodowe Centrum Nauki, 2016/22/E/NZ7/00420, Janusz Dabrowski.

Data availability Not applicable.

Declarations

Conflict of interest All authors have no conflicts of interest.

References

1. Aslam, B., Khurshid, M., Arshad, M. I., Muzammil, S., Rasool, M., Yasmeen, N., et al. (2021). Antibiotic resistance: One health one world outlook. *Frontiers in Cellular and Infection Microbiology, 11*, 771510.
2. World Health Organization (2015). *Global action plan on antimicrobial resistance*, WHO Library Cataloguing-in-Publication Data, ISBN: 9789241509763.
3. Talebi Bezmin Abadi, A., Rizvanov, A. A., Haertlé, T., & Blatt, N. L. (2019). World Health Organization report: Current crisis of antibiotic resistance. *BioNanoScience, 9*, 778–788.
4. Wainwright, M. (2020). A new penicillin? *Antibiotics, 9*(3), 117.
5. Blair, J. M., Webber, M. A., Baylay, A. J., Ogbolu, D. O., & Piddock, L. J. (2015). Molecular mechanisms of antibiotic resistance. *Nature Reviews Microbiology, 13*(1), 42–51.
6. Ghosh, C., Sarkar, P., Issa, R., & Haldar, J. (2019). Alternatives to conventional antibiotics in the era of antimicrobial resistance. *Trends in Microbiology, 27*(4), 323–338.
7. Cooper, R., & Kirketerp-Møller, K. (2018). Non-antibiotic antimicrobial interventions and antimicrobial stewardship in wound care. *Journal of Wound Care, 27*(6), 355–377.
8. Pucelik, B., & Dąbrowski, J. M. (2022). Photodynamic inactivation (PDI) as a promising alternative to current pharmaceuticals for the treatment of resistant microorganisms. *Advances in Inorganic Chemistry, 79*, 65–108.
9. Santos, P., Gomes, A. T., Lourenço, L. M., Faustino, M. A., Neves, M. G., & Almeida, A. (2022). Anti-viral photodynamic inactivation of T4-like bacteriophage as a mammalian virus model in blood. *International Journal of Molecular Sciences, 23*(19), 11548.
10. Almeida, A., Faustino, M. A. F., & Neves, M. G. (2020). Antimicrobial photodynamic therapy in the control of COVID-19. *Antibiotics, 9*(6), 320.
11. Cieplik, F., Deng, D., Crielaard, W., Buchalla, W., Hellwig, E., Al-Ahmad, A., et al. (2018). Antimicrobial photodynamic therapy–what we know and what we don't. *Critical Reviews in Microbiology, 44*(5), 571–589.
12. Gulías, Ò., McKenzie, G., Bayó, M., Agut, M., & Nonell, S. (2020). Effective photodynamic inactivation of 26 Escherichia coli strains with different antibiotic susceptibility profiles: A planktonic and biofilm study. *Antibiotics, 9*(3), 98.
13. Wainwright, M., Maisch, T., Nonell, S., Plaetzer, K., Almeida, A., Tegos, G. P., et al. (2017). Photoantimicrobials—Are we afraid of the light? *The Lancet Infectious Diseases, 17*(2), e49–e55.
14. Ragas, X., Sanchez-Garcia, D., Ruiz-González, R., Dai, T., Agut, M., Hamblin, M. R., et al. (2010). Cationic porphycenes as potential photosensitizers for antimicrobial photodynamic therapy. *Journal of Medicinal Chemistry, 53*(21), 7796–7803.
15. Wainwright, M. (2018). Synthetic, small-molecule photoantimicrobials–A realistic approach. *Photochemical & Photobiological SCIENCES, 17*, 1767–1779.
16. Dąbrowski, J. M., Pucelik, B., Regiel-Futyra, A., Brindell, M., Mazuryk, O., Kyzioł, A., et al. (2016). Engineering of relevant photodynamic processes through structural modifications of metallotetrapyrrolic photosensitizers. *Coordination Chemistry Reviews, 325*, 67–101.
17. Alves, E., Faustino, M. A., Neves, M. G., Cunha, A., Nadais, H., & Almeida, A. (2015). Potential applications of porphyrins in photodynamic inactivation beyond the medical scope. *Journal of Photochemistry and Photobiology C: Photochemistry Reviews, 22*, 34–57.
18. Vinagreiro, C. S., Zangirolami, A., Schaberle, F. A., Nunes, S. C., Blanco, K. C., Inada, N. M., et al. (2020). Antibacterial photodynamic inactivation of antibiotic-resistant bacteria and biofilms with nanomolar photosensitizer concentrations. *ACS Infectious Diseases, 6*(6), 1517–1526.
19. Aroso, R. T., Dias, L. D., Blanco, K. C., Soares, J. M., Alves, F., da Silva, G. J., et al. (2022). Synergic dual phototherapy: Cationic imidazolyl photosensitizers and ciprofloxacin for eradication of in vitro and in vivo E. coli infections. *Journal of Photochemistry and Photobiology B: Biology, 233*, 112499.
20. Huang, L., El-Hussein, A., Xuan, W., & Hamblin, M. R. (2018). Potentiation by potassium iodide reveals that the anionic porphyrin TPPS4 is a surprisingly effective photosensitizer for antimicrobial photodynamic inactivation. *Journal of Photochemistry and Photobiology B: Biology, 178*, 277–286.
21. Pucelik, B., Paczyński, R., Dubin, G., Pereira, M. M., Arnaut, L. G., & Dąbrowski, J. M. (2017). Properties of halogenated and sulfonated porphyrins relevant for the selection of photosensitizers in anticancer and antimicrobial therapies. *PLoS ONE, 12*(10), e0185984.
22. Revuelta-Maza, M. Á., González-Jiménez, P., Hally, C., Agut, M., Nonell, S., de la Torre, G., et al. (2020). Fluorine-substituted tetracationic ABAB-phthalocyanines for efficient photodynamic inactivation of Gram-positive and Gram-negative bacteria. *European Journal of Medicinal Chemistry, 187*, 111957.
23. Arnaut, L. G., Pereira, M. M., Dąbrowski, J. M., Silva, E. F., Schaberle, F. A., Abreu, A. R., et al. (2014). Photodynamic therapy efficacy enhanced by dynamics: The role of charge transfer and photostability in the selection of photosensitizers. *Chemistry–A European Journal, 20*(18), 5346–5357.
24. Pucelik, B., Sułek, A., Drozd, A., Stochel, G., Pereira, M. M., Pinto, S. M., et al. (2020). Enhanced cellular uptake and photodynamic effect with amphiphilic fluorinated porphyrins: The role of sulfoester groups and the nature of reactive oxygen species. *International Journal of Molecular Sciences, 21*(8), 2786.
25. Goslinski, T., & Piskorz, J. (2011). Fluorinated porphyrinoids and their biomedical applications. *Journal of Photochemistry and Photobiology C: Photochemistry Reviews, 12*(4), 304–321.
26. Pandurang, T. P., Cacaccio, J., Durrani, F. A., Dukh, M., Alsaleh, A. Z., Sajjad, M., et al. (2023). A remarkable difference in pharmacokinetics of fluorinated versus iodinated photosensitizers derived from chlorophyll-a and a direct correlation between the tumor uptake and anti-cancer activity. *Molecules, 28*(9), 3782.
27. Revuelta-Maza, M. A., Nonell, S., De La Torre, G., & Torres, T. (2019). Boosting the singlet oxygen photosensitization abilities of Zn (ii) phthalocyanines through functionalization with bulky fluorinated substituents. *Organic & Biomolecular Chemistry, 17*(32), 7448–7454.
28. Dąbrowski, J. M., Pucelik, B., Pereira, M. M., Arnaut, L. G., & Stochel, G. (2015). Towards tuning PDT relevant photosensitizer properties: Comparative study for the free and Zn2+ coordinated meso-tetrakis [2, 6-difluoro-5-(N-methylsulfamylo) phenyl] porphyrin. *Journal of Coordination Chemistry, 68*(17–18), 3116–3134.
29. Deng, J., Li, H., Yang, M., & Wu, F. (2020). Palladium porphyrin complexes for photodynamic cancer therapy: Effect of porphyrin units and metal. *Photochemical & Photobiological Sciences, 19*, 905–912.

30. Kee, H. L., Bhaumik, J., Diers, J. R., Mroz, P., Hamblin, M. R., Bocian, D. F., et al. (2008). Photophysical characterization of imidazolium-substituted Pd (II), In (III), and Zn (II) porphyrins as photosensitizers for photodynamic therapy. *Journal of Photochemistry and Photobiology A: Chemistry, 200*(2–3), 346–355.
31. Mroz, P., Bhaumik, J., Dogutan, D. K., Aly, Z., Kamal, Z., Khalid, L., et al. (2009). Imidazole metalloporphyrins as photosensitizers for photodynamic therapy: Role of molecular charge, central metal and hydroxyl radical production. *Cancer Letters, 282*(1), 63–76.
32. Xuan, W., Huang, L., Wang, Y., Hu, X., Szewczyk, G., Huang, Y. Y., et al. (2019). Amphiphilic tetracationic porphyrins are exceptionally active antimicrobial photosensitizers: In vitro and in vivo studies with the free-base and Pd-chelate. *Journal of Biophotonics, 12*(8), e201800318.
33. Dąbrowski, J. M., Pucelik, B., Pereira, M. M., Arnaut, L. G., Macyk, W., & Stochel, G. (2015). New hybrid materials based on halogenated metalloporphyrins for enhanced visible light photocatalysis. *RSC Advances, 5*(113), 93252–93261.
34. Azzouzi, A.-R., Lebdai, S., Benzaghou, F., & Stief, C. (2015). Vascular-targeted photodynamic therapy with TOOKAD® Soluble in localized prostate cancer: Standardization of the procedure. *World Journal of Urology, 33*, 937–944.
35. Scherz, A., & Salomon, Y. (2013). The story of Tookad: From bench to bedside*, Handbook of Photomedicine*, Taylor & Francis eBook, 459–474, ISBN: 9780429193842.
36. Hamblin, M. R., & Hasan, T. (2004). Photodynamic therapy: A new antimicrobial approach to infectious disease? *Photochemical & Photobiological Sciences, 3*(5), 436–450.
37. Sułek, A., Pucelik, B., Kobielusz, M., Barzowska, A., & Dąbrowski, J. M. (2020). Photodynamic inactivation of bacteria with porphyrin derivatives: Effect of charge, lipophilicity, ROS generation, and cellular uptake on their biological activity in vitro. *International Journal of Molecular Sciences, 21*(22), 8716.
38. Silva, J. N., Silva, A. M., Tomé, J. P., Ribeiro, A. O., Domingues, M. R. M., Cavaleiro, J. A., et al. (2008). Photophysical properties of a photocytotoxic fluorinated chlorin conjugated to four β-cyclodextrins. *Photochemical & Photobiological Sciences, 7*(7), 834–843.
39. Ribeiro, C. P., Faustino, M. A., Almeida, A., & Lourenço, L. M. (2022). The Antimicrobial photoinactivation effect on Escherichia coli through the action of inverted cationic porphyrin-cyclodextrin conjugates. *Microorganisms, 10*(4), 718.
40. Ribeiro, C. P., Gamelas, S. R., Faustino, M. A., Gomes, A. T., Tome, J. P., Almeida, A., et al. (2020). Unsymmetrical cationic porphyrin-cyclodextrin bioconjugates for photoinactivation of Escherichia coli. *Photodiagnosis and Photodynamic Therapy, 31*, 101788.
41. Moret, F., Gobbo, M., & Reddi, E. (2015). Conjugation of photosensitisers to antimicrobial peptides increases the efficiency of photodynamic therapy in cancer cells. *Photochemical & Photobiological Sciences, 14*, 1238–1250.
42. Tomé, J. P., Neves, M. G., Tomé, A. C., Cavaleiro, J. A., Soncin, M., Magaraggia, M., et al. (2004). Synthesis and antibacterial activity of new poly-S-lysine—Porphyrin conjugates. *Journal of Medicinal Chemistry, 47*(26), 6649–6652.
43. Castro, K. A., Moura, N. M., Figueira, F., Ferreira, R. I., Simoes, M. M., Cavaleiro, J. A., et al. (2019). New materials based on cationic porphyrins conjugated to chitosan or titanium dioxide: Synthesis, characterization and antimicrobial efficacy. *International Journal of Molecular Sciences, 20*(10), 2522.
44. Braz, M., Salvador, D., Gomes, A. T., Mesquita, M. Q., Faustino, M. A. F., Neves, M. G. P., et al. (2020). Photodynamic inactivation of methicillin-resistant Staphylococcus aureus on skin using a porphyrinic formulation. *Photodiagnosis and Photodynamic Therapy, 30*, 101754.
45. Vieira, C., Gomes, A. T., Mesquita, M. Q., Moura, N. M., Neves, M. G. P., Faustino, M. A. F., et al. (2018). An insight into the potentiation effect of potassium iodide on aPDT efficacy. *Frontiers in Microbiology, 9*, 2665.
46. Trochowski, M., Kobielusz, M., Pucelik, B., Dąbrowski, J. M., & Macyk, W. (2023). Dihydroxyanthraquinones as stable and cost-effective TiO2 photosensitizers for environmental and biomedical applications. *Journal of Photochemistry and Photobiology A: Chemistry, 438*, 114517.
47. Sułek, A., Pucelik, B., Kobielusz, M., Łabuz, P., Dubin, G., & Dąbrowski, J. M. (2019). Surface modification of nanocrystalline TiO2 materials with sulfonated porphyrins for visible light antimicrobial therapy. *Catalysts, 9*(10), 821.
48. Sułek, A., Pucelik, B., Kuncewicz, J., Dubin, G., & Dąbrowski, J. M. (2019). Sensitization of TiO2 by halogenated porphyrin derivatives for visible light biomedical and environmental photocatalysis. *Catalysis Today, 335*, 538–549.
49. Pinto, S. M., Vinagreiro, C. S., Tomé, V. A., Piccirillo, G., Damas, L., Pereira, M. M. (2019) Nitrobenzene method: A keystone in meso-substituted halogenated porphyrin synthesis and applications. *Journal of Porphyrins and Phthalocyanines, 23*(04n05), 329–346.
50. Dąbrowski, J. M., Pereira, M. M., Arnaut, L. G., Monteiro, C. J., Peixoto, A. F., Karocki, A., et al. (2007). Synthesis, photophysical studies and anticancer activity of a new halogenated water-soluble porphyrin. *Photochemistry and Photobiology, 83*(4), 897–903.
51. He, C., He, Q., Deng, C., Shi, L., Zhu, D., Fu, Y., et al. (2010). Turn on fluorescence sensing of vapor phase electron donating amines via tetraphenylporphyrin or metallophenylporphrin doped polyfluorene. *Chemical Communications, 46*(40), 7536–7538.
52. Ishii, K. (2012). Functional singlet oxygen generators based on phthalocyanines. *Coordination Chemistry Reviews, 256*(15–16), 1556–1568.
53. Dąbrowski, J. M. (2017). Reactive oxygen species in photodynamic therapy: Mechanisms of their generation and potentiation. *Advances in Inorganic Chemistry, 70*, 343–394.
54. Ragàs, X., Jiménez-Banzo, A., Sánchez-García, D., Batllori, X., & Nonell, S. (2009). Singlet oxygen photosensitisation by the fluorescent probe Singlet Oxygen Sensor Green®. *Chemical Communications, 20*, 2920–2922.
55. Aroso, R. T., Calvete, M. J., Pucelik, B., Dubin, G., Arnaut, L. G., Pereira, M. M., et al. (2019). Photoinactivation of microorganisms with sub-micromolar concentrations of imidazolium metallophthalocyanine salts. *European Journal of Medicinal Chemistry, 184*, 111740.
56. Rapacka-Zdończyk, A., Woźniak, A., Michalska, K., Pierański, M., Ogonowska, P., Grinholc, M., et al. (2021). Factors determining the susceptibility of bacteria to antibacterial photodynamic inactivation. *Frontiers in Medicine, 8*, 642609.
57. Wakeman, C. A., Stauff, D. L., Zhang, Y., & Skaar, E. P. (2014). Differential activation of Staphylococcus aureus heme detoxification machinery by heme analogues. *Journal of Bacteriology, 196*(7), 1335–1342.
58. Morales-de-Echegaray, A. V., Maltais, T. R., Lin, L., Younis, W., Kadasala, N. R., Seleem, M. N., et al. (2018). Rapid uptake and photodynamic inactivation of staphylococci by Ga (III)-protoporphyrin IX. *ACS Infectious Diseases, 4*(11), 1564–1573.
59. Reynoso, E., Ferreyra, D. D., Durantini, E. N., & Spesia, M. B. (2019). Photodynamic inactivation to prevent and disrupt Staphylococcus aureus biofilm under different media conditions. *Photodermatology, Photoimmunology & Photomedicine, 35*(5), 322–331.
60. Gingichashvili, S., Feuerstein, O., & Steinberg, D. (2020). Topography and expansion patterns at the biofilm-agar interface in bacillus subtilis biofilms. *Microorganisms, 9*(1), 84.

61. Zheng, S., Bawazir, M., Dhall, A., Kim, H.-E., He, L., Heo, J., et al. (2021). Implication of surface properties, bacterial motility, and hydrodynamic conditions on bacterial surface sensing and their initial adhesion. *Frontiers in Bioengineering and Biotechnology, 9*, 643722.
62. Edwards, A. M., Potter, U., Meenan, N. A., Potts, J. R., & Massey, R. C. (2011). Staphylococcus aureus keratinocyte invasion is dependent upon multiple high-affinity fibronectin-binding repeats within FnBPA. *PLoS ONE, 6*(4), e18899.
63. Velazquez-Meza, M. E., Galarde-López, M., Carrillo-Quiróz, B., & Alpuche-Aranda, C. M. (2022). Antimicrobial resistance: One health approach. *Veterinary World, 15*(3), 743.
64. Wainwright, M. (2021). Anti-infective dyes in the time of COVID. *Dyes and Pigments, 196*, 109813.
65. Kawczyk-Krupka, A., Pucelik, B., Międzybrodzka, A., Sieroń, A. R., & Dąbrowski, J. M. (2018). Photodynamic therapy as an alternative to antibiotic therapy for the treatment of infected leg ulcers. *Photodiagnosis and Photodynamic Therapy, 23*, 132–143.
66. Pucelik, B., Sułek, A., & Dąbrowski, J. M. (2020). Bacteriochlorins and their metal complexes as NIR-absorbing photosensitizers: Properties, mechanisms, and applications. *Coordination Chemistry Reviews, 416*, 213340.
67. Beyene, B. B., Mihirteu, A. M., Ayana, M. T., & Yibeltal, A. W. (2020). Synthesis, characterization and antibacterial activity of metalloporphyrins: Role of central metal ion. *Results in Chemistry, 2*, 100073.
68. Skwor, T. A., Klemm, S., Zhang, H., Schardt, B., Blaszczyk, S., & Bork, M. A. (2016). Photodynamic inactivation of methicillin-resistant Staphylococcus aureus and Escherichia coli: A metalloporphyrin comparison. *Journal of Photochemistry and Photobiology B: Biology, 165*, 51–57.
69. Stojiljkovic, I., Evavold, B. D., & Kumar, V. (2001). Antimicrobial properties of porphyrins. *Expert Opinion on Investigational Drugs, 10*(2), 309–320.
70. Yang, E., Diers, J. R., Huang, Y. Y., Hamblin, M. R., Lindsey, J. S., Bocian, D. F., et al. (2013). Molecular electronic tuning of photosensitizers to enhance photodynamic therapy: Synthetic dicyanobacteriochlorins as a case study. *Photochemistry and Photobiology, 89*(3), 605–618.
71. Lazzeri, D., Rovera, M., Pascual, L., & Durantini, E. N. (2004). Photodynamic studies and photoinactivation of Escherichia coli Using meso-substituted cationic porphyrin derivatives with asymmetric charge distribution¶. *Photochemistry and Photobiology, 80*(2), 286–293.
72. Zorlu, Y., Dumoulin, F., Durmuş, M., & Ahsen, V. (2010). Comparative studies of photophysical and photochemical properties of solketal substituted platinum (II) and zinc (II) phthalocyanine sets. *Tetrahedron, 66*(17), 3248–3258.
73. Ziental, D., Mlynarczyk, D. T., Kolasinski, E., Güzel, E., Dlugaszewska, J., Popenda, Ł, et al. (2022). Zinc (II), palladium (II), and metal-free phthalocyanines bearing nipagin-functionalized substituents against Candida auris and selected multidrug-resistant microbes. *Pharmaceutics, 14*(8), 1686.
74. De Melo, W. C., Avci, P., De Oliveira, M. N., Gupta, A., Vecchio, D., Sadasivam, M., et al. (2013). Photodynamic inactivation of biofilm: Taking a lightly colored approach to stubborn infection. *Expert Review of Anti-Infective Therapy, 11*(7), 669–693.